2019

UNDERSTANDING THE STRUCTURE-PROPERTY-PERFORMANCE RELATIONSHIP OF SILICON NEGATIVE ELECTRODES

Jiazhi Hu
University of Kentucky, jz.hu@uky.edu
Author ORCID Identifier:
https://orcid.org/0000-0001-9102-9252
Digital Object Identifier: https://doi.org/10.13023/etd.2019.414

STUDENT AGREEMENT:

I represent that my thesis or dissertation and abstract are my original work. Proper attribution has been given to all outside sources. I understand that I am solely responsible for obtaining any needed copyright permissions. I have obtained needed written permission statement(s) from the owner(s) of each third-party copyrighted matter to be included in my work, allowing electronic distribution (if such use is not permitted by the fair use doctrine) which will be submitted to UKnowledge as Additional File.

I hereby grant to The University of Kentucky and its agents the irrevocable, non-exclusive, and royalty-free license to archive and make accessible my work in whole or in part in all forms of media, now or hereafter known. I agree that the document mentioned above may be made available immediately for worldwide access unless an embargo applies.

I retain all other ownership rights to the copyright of my work. I also retain the right to use in future works (such as articles or books) all or part of my work. I understand that I am free to register the copyright to my work.

REVIEW, APPROVAL AND ACCEPTANCE

The document mentioned above has been reviewed and accepted by the student's advisor, on behalf of the advisory committee, and by the Director of Graduate Studies (DGS), on behalf of the program; we verify that this is the final, approved version of the student's thesis including all changes required by the advisory committee. The undersigned agree to abide by the statements above.

Jiazhi Hu, Student

Dr. Yang-Tse Cheng, Major Professor

Dr. Matthew Beck, Director of Graduate Studies

UNDERSTANDING THE STRUCTURE-PROPERTY-PERFORMANCE RELATIONSHIP OF SILICON NEGATIVE ELECTRODES

DISSERTATION

A dissertation submitted in partial fulfillment of the
requirements for the degree of Doctor of Philosophy in the
College of Engineering
at the University of Kentucky

By

Jiazhi Hu

Lexington, Kentucky

Co- Directors: Dr. Yang-Tse Cheng, Professor of Materials Engineering

and Dr. Dibakar Bhattacharyya, Professor of Chemical Engineering

Lexington, Kentucky

2019

[https://orcid.org/0000-0001-9102-9252]

ABSTRACT OF DISSERTATION

UNDERSTANDING THE STRUCTURE-PROPERTY-PERFORMANCE RELATIONSHIP OF SILICON NEGATIVE ELECTRODES

Rechargeable lithium ion batteries (LIBs) have long been used to power not only portable devices, e.g., mobile phones and laptops, but also large scale systems, e.g., electrical grid and electric vehicles. To meet the ever increasing demand for renewable energy storage, tremendous efforts have been devoted to improving the energy/power density of LIBs. Known for its high theoretical capacity (4200 mAh/g), silicon has been considered as one of the most promising negative electrode materials for high-energy-density LIBs. However, diffusion-induced stresses can cause fracture and, consequently, rapid degradation in the electrochemical performance of Si-based negative electrodes. To mitigate the detrimental effects of the large volume change, several strategies have been proposed. This dissertation focuses on two promising approaches to make high performance and durable Si electrodes for high capacity LIBs.

First, the effect of polymeric binders on the performance of Si-based electrodes is investigated. By studying two types of polymeric binders, polyvinylidene fluoride (PVDF) and sodium alginate (SA) using peel tests, SEM, XPS, and FTIR, I show that the high cohesive strength at the binder-silicon interface is responsible for the superior cell performance of the Si electrodes with SA as a binder. Hydrogen bonds formed between SA and Si is the main reason for the high cohesive strength since neither PVDF nor SA bonds covalently with Si.

Second, the fabrication of high performance Si/polyacrylonitrile (PAN) composite electrode via oxidative pyrolysis is investigated. We show that high performance Si/polyacrylonitrile (PAN) composite negative electrodes can be fabricated by a robust heat treatment in air at a temperature between 250 and 400^{o}C. Using Raman, SEM, XPS, TEM, TGA, and nanoindention, we established that oxidation, dehydration, aromatization, and intermolecular crosslinking take place in PAN during the heat treatment, resulting in a stable cyclized structure which functions as both a binder and a conductive agent in the Si/PAN composite electrodes. With a Si mass loading of 1 mg/cm^{2}, a discharge capacity of ~1600 mAh/g at the 100th cycle is observed in the 400^{o}C treated Si/PAN composite electrode when cycled at a rate of C/3.

These studies on the structure-property-performance relations of Si based negative electrode may benefit the LIB community by providing (1) a guide for the design and optimization of binder materials for Si electrodes and (2) a facile method of synthesizing Si-based composite negative electrodes that can potentially be applied to other Si/polymer

systems for further increasing the power/energy density and lower the cost of LIBs for electric vehicle applications and beyond.

KEYWORDS: Lithium ion batteries, Si electrodes, performance, structure

Jiazhi Hu

(Name of Student)

07/01/2019

Date

UNDERSTANDING THE STRUCTURE-PROPERTY-PERFORMANCE RELATIONSHIP OF SILICON NEGATIVE ELECTRODES

By
Jiazhi Hu

Yang-Tse Cheng
Co-Director of Dissertation

Dibakar Bhattacharyya
Co-Director of Dissertation

Matthew Beck
Director of Graduate Studies

07/01/2019
Date

Dedicated To My Wonderful Mother

ACKNOWLEDGMENTS

My last four year's graduate study and life at UK have been enriched by interactions with many people. I appreciate everyone deeply.

My advisor, Prof. Yang-Tse Cheng, has been my role model by being kind, encouraging, knowledgeable, considerate, enthusiastic, and curious about everything. My research would be impossible and I wouldn't have gone this far without his support and understanding. I enjoyed and will miss the delightful, inspiring, and fruitful discussions with him. I am profoundly grateful to Dr. Xiaosong Huang of GM R&D Center, whom I worked with at GM R&D Center as a Visiting Scientist. Dr. Huang not only guided my research and spent much time to discuss numerous problems with me but also cared a lot about my life and career. I would like to thank Professor Dibakar Bhattacharyya, who has been my co-advisor in the last four years and provided incalculable support to my research. Next, I would like to thank Professors Jian Shi and Stephen Rankin for serving as my dissertation committee members and Professor Kozo Saito for being my outside examiner.

My sincere thanks also go to former and current group members: Dr. Jiagang Xu, Dr. Qinglin Zhang, Dr. Jie Pan, Dr. Tao Chen, Dr. Baleegh S Alobaid, Dr. Yan Sun, Dr. Xiaowen Zhan, Dr. Shuang Gao, Dr. Yikai Wang, Long Zhang, Ming Wang, and Andrew W. Meyer for their great help and friendship. In addition, I would like to thank other colleagues and stuff members: Dr. Dali Qian, Dr. Nicolas Briot, Nancy Miller, and Nick Cprek for their assistance and instrumental support. I would also like to thank my collaborators, Namal Wanninayake, Dr. Andrew Colburn, and Professor Doo Young Kim at UK, Nicole Ellison, Michael P. Balogh, and Dr. Xingcheng Xiao at General Motors,

Dr. Wensheng He, Dr. Steven Baxter, and Dr. Ramin Amin-Sanayei from Arkema for the helpful discussions and technical support.

I also received equally important support from family and friends. A very special gratitude goes to my sister, Jiahui Hu, who has been my best friend since I was born, for always providing me with unconditional and priceless love and support.

Finally, I would like to thank National Science Foundation (Award number 1355438) for the financial support.

TABLE OF CONTENTS

LIST OF TABLES

LIST OF FIGURES

Chapter 1 Introduction

1.1 A brief history of lithium ion batteries (LIBs)

Since the Industrial Revolution, people's life has been changed dramatically owing to the huge progress achieved in various scientific and technological fields, which were largely driven by the discovery and exploitation of fossil fuels. However, this energy resource is non-renewable and will be depleted in several hundred years. Furthermore, burning of carbonaceous fuels generates a large amount of CO_2, causing global warming, and putting all human beings in danger. Alternative energy sources to fossil fuels are urgently required. Electricity from renewable sources is one of the most promising candidates. Once stored in batteries, electricity can be used when and where it is needed. The applications of batteries cover almost every aspect of life. For example, batteries can be used as the back-up energy supply for electric grid, and power sources for electric vehicles or portable devices such as cellular phones and laptop computers. Among various batteries, LIB is one of the most attractive types. First commercialized in the late 1960s, the primary lithium based batteries were built using non-aqueous electrolyte, lithium metal negative electrode, and, predominantly, MnO_2 positive electrode[1]. Their high voltage, high energy density, and good stability over a wide temperature range generated ample interests. However, the dendrites formed from the lithium metal side in the charging process could penetrate through the separator, short the internal circuit, and cause safety problem, which greatly limited the application of primary lithium based cells[2]. Research on the lithium based batteries continued and a major breakthrough occurred in 1991. In that year, a secondary (rechargeable) LIB using graphite negative electrode and $LiCoO_2$ positive electrode was introduced to the market by Sony. Fig. 1.1[3] shows how this battery

works. During the charging process, lithium ions are driven by the applied voltage to move from the positive electrode, through the electrolyte, and intercalate into the graphite negative electrode. Simultaneously, the electrons transfer in the same direction through the external circuit. In the discharging process, both lithium ions and electrons move from the negative electrode to the positive electrode and power the devices that are connected to the battery. Compared with other batteries, e.g., lead acid and Ni-Cd batteries, LIBs have very high energy density in terms of both per unit weight and per unit volume as shown in Fig. 1.2[4]. Because dendrites formation is avoided by changing the negative electrode from lithium metal to graphite, LIBs have been used for many applications. However, great efforts have been devoted to improving the performance of LIBs to meet the ever increasing demanding for higher capacity and larger power density. A brief review of the related work will be discussed in more detail in this chapter.

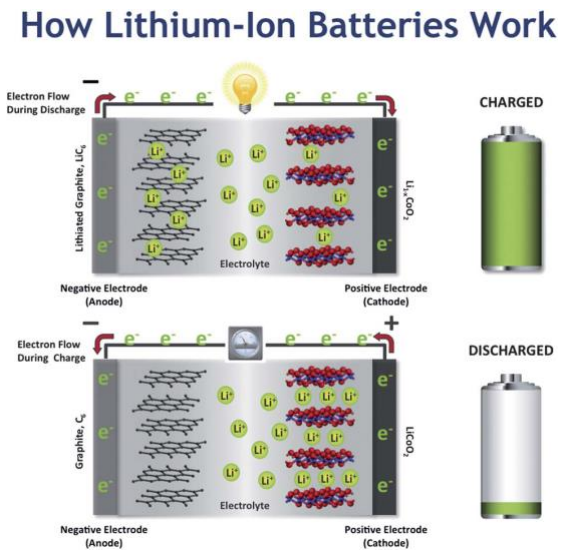

Figure 1.1 A schematic illustration of the working principle of LIBs[3]

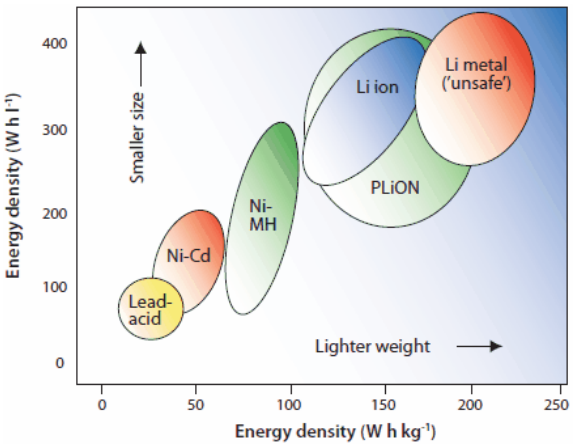

Figure 1.2 Comparison of the different battery technologies in terms of volumetric and gravimetric energy density[4]

1.2 Fabrication of electrodes

There are several ways of fabricating LIB electrodes. The most common or the traditional one is the slurry-coating method. Fig. 1.3[5] shows the schematic of this method. First, a slurry is made by mixing raw materials with solvent. Then, the slurry is cast onto a current collector (Cu in negative electrode while Al in positive electrode). After that, a drying process is conducted to remove the solvent and the dried electrode is sent through a roller press, also known as a calendering machine, to reduce the porosity and improve the adhesion between electrode layer and the current collector. Finally, the electrode is cut into desired sizes and shapes to fabricate various LIBs for different applications. The raw materials involved in the slurry-coating method are usually active material, conductive agent, and binder. Active material is the material that can reversibly store lithium. For example, the graphite and $LiCoO_2$ are the active materials in the respective negative and positive electrodes. The carbon black is the most common conductive agent used to improve the electronic conductivity of the electrode. Binder is usually a polymer, acting as a glue to bind the active material, conductive agent, and current collector. It has an

important role in producing batteries and improving their performance and durability. Styrene butadiene copolymer (SBR) and polyvinylidene fluoride (PVDF) are the most frequently used binders in the respective negative and positive electrode in commercial LIBs.

A binder-free method of making electrode is possible for certain materials and electrode designs [6]. The use of binder-free electrode could lower the weight and increase the energy density of LIBs. But the synthesis of active material is usually quite complicated compared to the traditional way and the cost has not been systematically studied.

A solvent-free dry powder coating process[7] has been demonstrated in several publications. In this method, active material, conductive agent, and binder are electrostatically sprayed onto the current collector without using any solvent. The cost of electrode fabrication process could be reduced by eliminating the drying process. Moreover, the absence of toxic solvent such as N-methylpyrrolidone (NMP, the solvent to dissolve PVDF) made the dry-powder coating process environmentally friendly.

The electrodes fabricated by the aforementioned three approaches are porous. Knowing the volume of the electrode, the density and mass of each material, the porosity of an electrode can be calculated by the following equation:

$$Porosity = \left(1 - \frac{\sum_i \frac{m_i}{\rho_i}}{V_{electrode}}\right) \times 100\%$$

where m_i is the mass and ρ_i is the density of the material i that is present in the electrode, e.g., i could be active material, conductive agent, and binder. $V_{electrode}$ is the volume of the electrode.

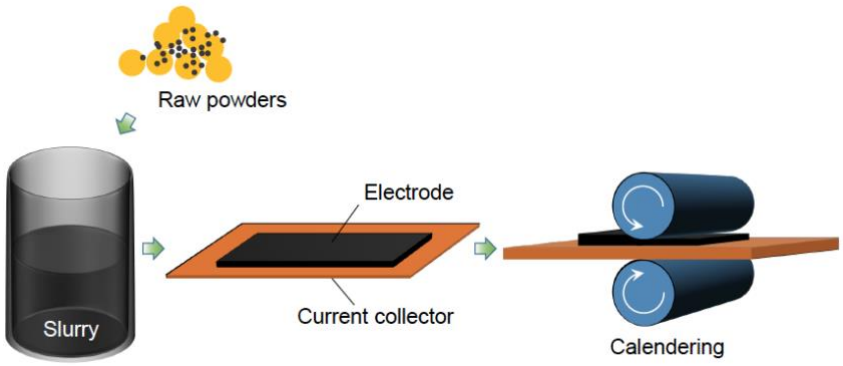

Figure 1.3 Schematic of fabricating electrodes for LIBs[5]

1.3 Cell Configuration

LIBs are generally used in four configurations: coin or button cell, prismatic cell, pouch cell, and cylindrical cell. Coin cell is a small single cell battery shaped as a squat cylinder with certain diameter and height. It is often used to power portable electronic devices such as wrist watches, car keys, and pocket calculators. It is also the most commonly used configuration in laboratory scale tests of the electrochemical performance of electrodes. As shown in the schematic diagram in Fig. 1.4[8], a typical coin cell consists of a casing bottom and a casing top as the respective positive terminal and the negative terminal. A positive electrode and a negative electrode are placed in between of the two terminals separated by a microporous film which allows lithium ions but not electrons to pass through. A stainless steel spacer and a disk spring are added in the cell to secure the electrodes. Organic carbonate electrolyte contains lithium salt is generally used in the cell to allow lithium ion transport.

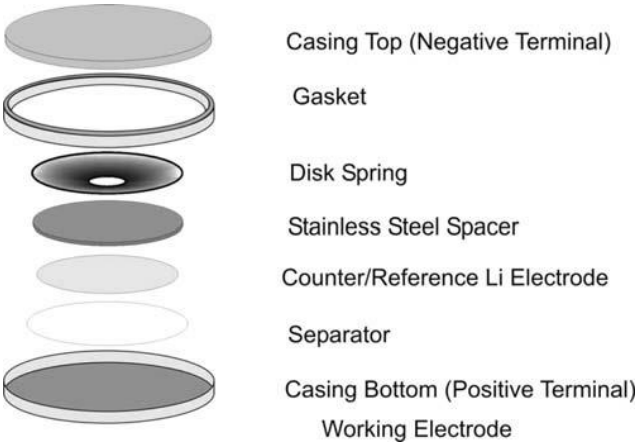

Figure 1.4 Structure of a coin cell[8]

1.4 Development of the negative electrode

1.4.1 Carbon-based electrode

Graphite is the first and is still the most commonly used negative electrode material in commercial LIBs. It has a layered structure, which consists of carbon atoms arranged in hexagonal rings. Between these layers, only weak van der Waals bonds exist[9]. It is well studied that different atoms or atomic groups can be intercalated in between the layers. For lithium, the intercalation process can be divided into two stages as shown in Fig. 1.5[10]. At the end of the lithiation process, one lithium atom is surrounded by six carbon atoms.

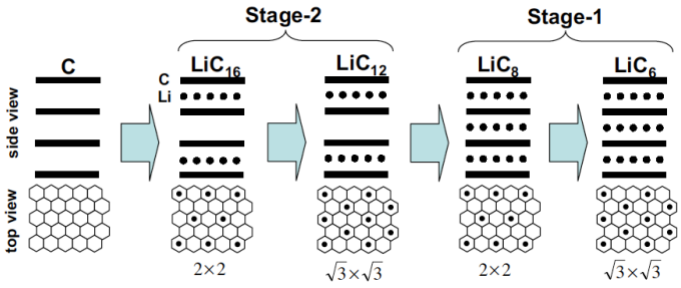

Figure 1.5 Li insertion process to graphite[10]

Once the lithiation mechanism is known, theoretical capacity of the active material can be calculated through the following equation:

$$Q_{Theoretical} = \frac{nF}{M} \quad (1)$$

where n is the number of charge carries, F is the Faraday constant, and M is the molecular weight of the active material. For graphite, n=1 and $M = 72$ g (6 mol×12 g/mol) at the fully lithiated state. The theoretical capacity of it is therefore:

$$Q_{Theoretical} = \frac{1mol \times 6.02 \times 10^{23} mol^{-1} \times 1.602 \times 10^{-19} C}{72g} = \frac{96440.4As}{72g}$$
$$= \frac{96440.4 \times 1000}{3600 \times 72} mAh/g = 372.07\, mAh/g$$

With the development of advanced synthesizing approaches, many forms of carbon-based materials have been investigated for LIB applications. Among them, graphene has attracted a lot of attention because of its extraordinary physical and mechanical properties. Several publications have reported that graphene sheets exhibited a specific capacity much higher than that of graphite[11-13]. One speculation is that lithium atoms not only locate between graphene layers but also position themselves at sites such as cavities, defects, and edges of graphene planes[14]. But the mechanism remains unclear. Another type of carbon material that has been intensively studied is carbon nanotubes. Envisioned as a rolled up graphene sheet or multiple sheets, carbon nanotubes can be categorized into single wall nanotube (SWNT) or multi walled carbon nanotube (MWNT)[15]. Ng *et al*. applied SWNT as negative electrode material in LIBs and found that the first discharge capacity can reach 1700 mAh/g, which is much higher than that of graphite. But the irreversible capacity in the first cycle is also enormous. Several reasons could be responsible, e.g., reduction of dioxygen molecules or the formation of solid electrolyte interphase (SEI). Although the cycling capability is poor, SWNT-based anodes are still being explored. Because of the "free standing" capability of SWNT, binder was not needed in the electrode. As a result, the weight of electrode could be reduced

significantly[16]. For MWNT, a ten times higher power density than that of conventional LIBs has been achieved with comparable capacity and excellent cycling stability[17].

1.4.2 Metal oxide electrode

Metal oxides have been widely studied as potential electrode materials in LIBs. Their ease of large-scale fabrication and rich redox reactions have attracted a great deal of interests[18]. Iron oxides, in the form of hollow nanoparticles[19], nanotubes[20], and nanoflakes[21], have been shown to be capable of delivering comparable capacity to graphite at relatively high voltage. NiO nanotubes showed a first discharge capacity as high as 600 mAh/g but rapidly decreased to and stabilized at 200 mAh/g after 10 cycles due to the formation of SEI[22]. TiO_2 nanotube showed excellent capacity retention after the first cycle, exhibiting only 4.5% capacity fade from 100^{th} to the 200^{th} cycle[23]. Co_3O_4 nanotubes, nanorods, and nanoparticles presented a specific capacity over 800 mAh/g at the end of the first lithiation process and maintained at greater than 450 mAh/g after 100 cycles[24]. For $CoMn_2O_4$, in the form of hollow microtubes, a superior first discharge capacity of 1282 mAh/g was obtained and retained at 624 mAh/g after 50 cycles[25]. Although the aforementioned metal-oxide electrodes have good capacity retention, the irreversible capacity loss in the first cycle is large, which must be overcome prior to practical applications[26].

1.4.3 Alloy electrode

It was first reported by Dey in 1971 that lithium could alloy with other metals in an organic electrolyte electrochemical cell[27]. Since then, Li-alloying reactions with various elements have been extensively investigated[28]. Many elements, e.g., Si, Sn, Sb, Al, Mg, and Ge, are found to form intermetallics with lithium[29]. The electrochemical process of

these Li-alloys is the lithium alloying in the charging process and lithium dealloying in the discharging process according to:

$$M + xLi^+ + xe^- \rightleftarrows Li_xM$$

Among the various Li alloy elements, Si has been considered one of the most promising negative electrode materials for the next generation LIBs. Si is abundant, cheap, environmental benign, and, most importantly, has the highest theoretical gravimetric and volumetric capacity as shown in Fig. 1.6[30]. The electrochemical reactions between Si and Li are as followed[31]:

$$\text{First lithiation: } c - Si \xrightarrow{+Li} a - Li_ySi \xrightarrow{+Li} a - Li_xSi \xrightarrow{+Li} c - Li_{15}Si_4$$

$$\text{First delithiation: } c - Li_{15}Si_4 \xrightarrow{-Li} a - Li_zSi \xrightarrow{-Li} a - Si$$

$$\text{Subsequent cycling: } a - Si \xrightarrow{+Li} a - Li_xSi \xrightarrow{+Li} c - Li_{15}Si_4$$

where “c” and “a” indicate a crystalline phase and amorphous phase, respectively.

At the beginning of the first lithiation, crystalline Si becomes amorphous and crystallizes into $Li_{15}Si_4$ at about 60 mV (vs Li/Li^+). At the beginning of first delithiation, $Li_{15}Si_4$ phase coexists with amorphous Li_zSi phase. With more Li extraction, $Li_{15}Si_4$ phase gradually disappears, the amorphous phase persists. The subsequent cycling is the phase transformation between amorphous Si and crystalline $Li_{15}Si_4$ with an intermediate amorphous Li_xSi phase. When four silicon atoms react with fifteen lithium atoms, a theoretical specific capacity of 3579 mAh/g is reached, which is about ten times higher than that of graphite. However, accompanied with the exceptional high capacity is a volume expansion as large as 300%. The remarkable volume change generates large stress in Si, leading to particle fracture, which was confirmed by *in situ* transmission electron microscope (TEM) observation[32] and acoustic emission studies[33]. The fracture could

further induce pulverization of Si, causing electrically isolation and continuous growth of SEI. Thus, Si electrodes have poor reversibility and cycling stability.

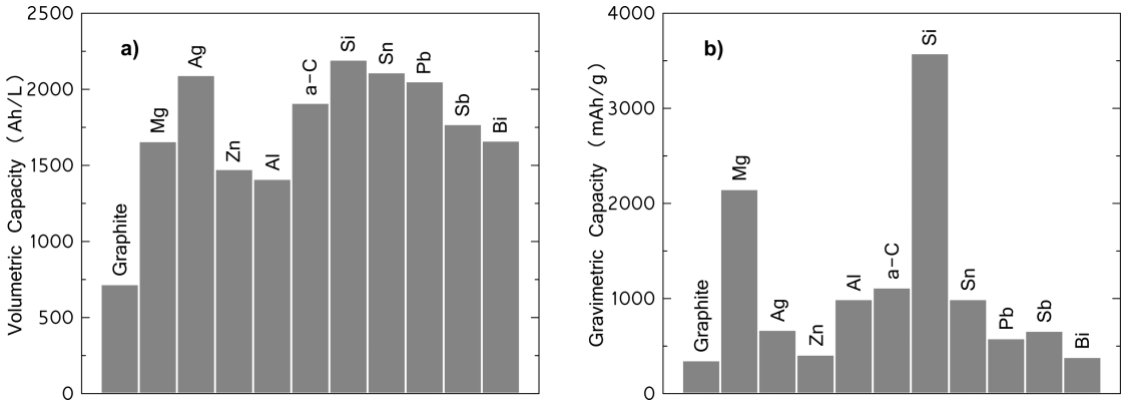

Figure 1.6 (a) Volumetric capacities calculated at the state of full lithiation and (b) gravimetric capacities of selected elements[30]

It was first predicted by Huggins *et al.* that there should be a critical particle size below which particle fracture would not occur upon cycling[34], which may explain the finding in early studies that with nano-sized Si as active material the cycling performance improved significantly[13, 35-39]. Subsequent modeling and experimental investigations indicated that there is a critical size of approximately 300 nm and 150 nm for Si nano-wires[40] and Si nano-particles[41], respectively, under which fracture during lithiation is avoided. Based on this discovery, various nano morphologies including yolk-shell structure[42, 43], nanotube[44-46], nanowire [47-50], and nano flake[51], have been developed to further improve the cycling performance and durability of Si based electrodes.

Porous structures have also been of great interest because the large voids could provide space for volume expansion and thus maintain the structure integrity during lithiation of Si. Initial attempts conducted by Kim *et al.* demonstrated that, by using 3D porous Si particles as active material, the composite electrode delivered a specific capacity higher than 2400 mAh/g after cycled at a rate of 0.2C for 100 cycles[52]. Thenceforth,

continuing efforts have been devoted to synthesizing porous Si via diverse ways, including aluminothermic reduction[53, 54], magnesiothermic reduction[55-60], etching method[61-69], and solvothermal reaction[70].

1.4.4 Composite electrode

Since each electrode material has its own advantages and disadvantages, putting different electrode materials together to form composite electrodes may be able to overcome the weaknesses from individual components and improve the performance of LIBs. A common approach to prepare composite electrodes is to combine conductive additives with nanostructured electrode materials especially those with poor electronic conductivity[71]. C/Fe_3O_4 composite nanofibers exhibited a high reversible capacity of 1007 mAh/g at the 80_{th} cycle, which is much better than carbon nanofibers[72]. A nanoflake MnO_2/carbon nanotube composite electrode showed a reversible capacity of 801 mAh/g for the first 20 cycles with a good rate capability and no capacity fade[73]. A nanocomposite electrode consists of Co_3O_4 nanoparticles anchored on graphene sheet displays a reversible capacity up to 935 mAh/g after 30 cycles with over 98% coulombic efficiency[74]. For alloy electrodes, similar results have been reported. Composite electrodes prepared with Sn nanoparticles encapsulated in elastic hollow carbon spheres showed a capacity larger than 550 mAh/g after 100 cycles, as well as high volume capacity and good cycling performance[75]. Si/carbon nanotube[76-81], Si/graphene[82], and Si/carbon coating[83-87] composite electrodes all present superior electrochemical performance with large reversible capacity and long cycle life.

1.5 Development of positive electrode

As the first positive electrode material in commercial rechargeable LIBs, $LiCoO_2$ was introduced in 1980 by Professor Goodenough[88]. It has a layered rock salt structure, as shown in Fig. 1.7[89], where lithium ions can be reversibly inserted and removed. The typical operation voltage window for $LiCoO_2$ electrode is between 3 V to 4.2 V, corresponding to a capacity of 140 mAh/g[90]. Other layered lithium transition metal oxides isostructural with $LiCoO_2$ e.g. $LiNiO_2$[91] and $LiMnO_2$[92] have also been discovered favorable for lithium ion intercalation and extraction, and hence have become alternative positive electrode materials. However, subsequent studies revealed that exothermic oxidation of the organic electrolyte with delithiated Li_xNiO_2 occurred during cycling, which could cause safety problems[93]. $LiMnO_2$, on the other hand, has a severe capacity fading problem induced by not only the partial oxidation of manganese ions but also the migration of Mn ions into the interlayer lithium site during the electrochemical charge-discharge process[94]. Doping of $LiNiO_2$ or $LiMnO_2$ with transition metals has been proven as an effective strategy to increase structural stability and adjust chemical mismatch with lithium ion intercalation/extraction. As a one-to-one mixture of $LiNiO_2$ and $LiMnO_2$, $LiNi_{1/2}Mn_{1/2}O_2$ showed rechargeable capacity of 150 mAh/g when tested between 2.5 V and 4.3 V for 30 cycles[95]. Replacing some Co with Ni and Mn, the new material $LiNi_{1/3}Co_{1/3}Mn_{1/3}O_2$ exhibited close to 200 mAh/g rechargeable capacity with current as high as 1.6 A/g at a voltage window of 2.5 V-4.6 V[96]. To further increase the capacity, lower the cost, and reduce environment impact, Ni rich compounds, e.g., $LiNi_{0.6}Co_{0.2}Mn_{0.2}O_2$[97] and $LiNi_{0.75}Co_{0.10}Ni_{0.15}O_2$[98] were developed. However, with

increasing Ni content, capacity retention gradually decreases in these materials. Both thermal and electrochemical stability deteriorate as well[99].

Another type of positive electrode is the spinel lithium metal oxide. $LiMn_2O_4$, also introduced by Prof. Goodenough[100], has gained much attention owing to its low cost, high abundance, and environmental compatibility. Although the performance of $LiMn_2O_4$-based material has been improved, its rechargeable capacity is still lower than that of $LiCoO_2$[101].

The third widely studied positive electrode material has the ordered-olivine phosphate structure. Among the candidates, $LiFePO_4$ is one of the most attractive materials because of its low toxicity and relatively high theoretical specific capacity of 160 mAh/g. However, because of the lower operating voltage (3.5 V), the energy density of the LIBs using $LiFePO_4$ as positive electrode is less than the one consisting lithium transition metal oxide electrode when the same negative electrode is employed. In addition, the rate capability of $LiFePO_4$ electrode is poor due to the low electronic and low ionic conductivity. Carbon coating has been shown effective in improving the performance of $LiFePO_4$ electrode but it further lowers the energy density of the electrode simultaneously[102].

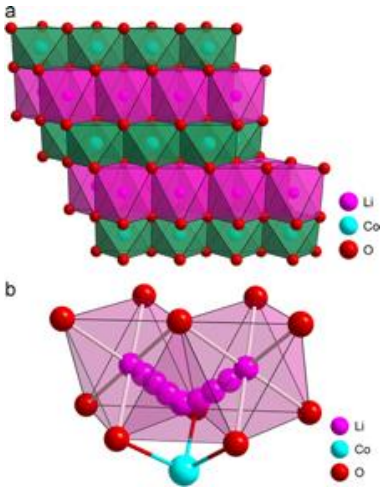

Figure 1.7 (a) Crystalline structure of layered LiCoO2 and (b) its corresponding lithium diffusion pathways[89]

1.6 Development of binder

Effective binders in an LIB should have several characteristics, e.g., excellent adhesion to the current collector, high melting point, good electron and lithium-ion conductivity, as well as the ability to produce a stable slurry viscosity during long term storage. However, no binder can meet all the criteria. Currently, PVDF and SBR are the most widely used binders in the positive and negative electrode, respectively.

PVDF has a simple structure with a monomer consists of two hydrogen atoms and two fluorine atoms (-CH_2-CF_2-). It has good thermal stability, abrasion and chemical resistance[103]. The main drawback of using PVDF as binder in LIBs is that the solvent used to dissolve PVDF is NMP, which is quite harmful to health. Decreasing or eliminating the use of NMP will be an important task. SBR is a general term for a copolymer that mainly consists of styrene and butadiene. It is stable at high temperature and can be dissolved in water.

For Si electrodes, polymeric binders with appropriate functional groups are expected to improve the performance vastly[104]. Several kinds of binders were developed and numerous investigations have revealed that the role of binder is crucial in achieving

the desired electrochemical performance and long-term cycling stability of Si-based electrodes. Because of the large volume change (>300%) during lithiation/delithiation, many researchers believe that binder with large extension before breaking could help improve the performance of Si-based electrodes. However, several studies reported that stiff binders, such as carboxymethyl cellulose (CMC) with only 5-8% reversible elongation, produced much better performance in Si electrodes than the elastomeric binders, such as PVDF whose elongation limit in strain is greater than 20%[105-108]. Other binders, e.g., polyacrylic acid (PAA)[109], nafion[110], and sodium alginate[111], have all been shown to work well in Si electrodes regardless of their own mechanical property. However, the mechanism is unclear, which is one of the primary motivations of this thesis.

Chapter 2 Effects of adhesion and cohesion on the electrochemical performance and durability of silicon electrodes

Most of the content of this chapter is duplicated from the paper published as ref. [112]: J. Z. Hu, Y. K. Wang, D, W, Li, and Y. T. Cheng, Effects of adhesion and cohesion on the electrochemical performance and durability of silicon composite electrodes. J. Power Sources, 397 (2018) 223-230.

2.1 Introduction

To meet the ever increasing demand in energy storage, tremendous efforts have been devoted to lithium ion battery (LIB) research[47]. Silicon, known for its high theoretical specific capacity (4200 mAh/g), has been intensively studied. Compared with the most commonly used graphite (372 mAh/g) electrode[113-115] in commercial LIBs, Si has the potential to become a negative electrode material for LIBs. However, volume expansion of Si particles can be larger than 300 % upon full lithiation, causing pulverization as well as delamination of the electrode layer from the current collector. As a result, the loss of electrical conducting network[116-119], the continuous growth of solid electrolyte interface (SEI)[120], poor reversibility, and rapidly faded electrochemical performance would occur, impeding the application of Si electrodes in LIBs.

A tether model proposed by Chen *et al*. showed that the capacity retention of amorphous alloy anodes with 125 % volume change was significantly improved by employing a binder with large extension before breakage and good adhesion strength with active material[121]. Si electrodes may also benefit from the same approach. However, several investigations demonstrated that stiff and brittle binders actually functioned better in Si electrodes than elastomeric binders with much larger elongation to failure[105-108].

Furthermore, a recent publication showed that, among the three binder materials that have been studied, the stiffest binder (sodium alginate) and the softest binder (nafion) both worked much better in Si electrodes than poly (vinylidene fluoride) PVDF, whose elastic modulus and hardness are in between that of sodium alginate and nafion[122]. Thus, the mechanical property of binder material alone does not necessarily correlate with the electrochemical performance of Si electrodes. Instead, the interaction between Si and polymeric binder may play a more important role.

The influence of a binder on the adhesion behavior of the electrode laminate on the current collector has also been considered important. Indeed, several studies reported that the employment of an adhesive binder could improve the electrochemical performance of Si electrodes by elevating the interfacial strength between electrode and current collector[123-127]. However, Kierzek pointed out, after comparing several binder systems, that the cycling stability was not necessarily enhanced by a higher adhesive strength between the electrode film and the current collector[128].

The adhesion behavior between electrode laminate and current collector may be quantified through a pull-off test according to Haselrider *et al*. They showed that several failure mechanisms exist in a pull-off test[129]. Depending on where the failure occurs, the measured pull-off stress could be either the adhesive strength between electrode layer and current collector or the cohesive strength within the electrode film. Thus, it is important to carry out detailed microstructure observation to properly interpret adhesion test results.

In the present work, the binder-Si interfacial strength and its influence on the durability of Si electrodes have been studied by carrying out peel tests, electrochemical performance measurements, chemical analysis, and microstructure observations. Our

results show that it is not the mechanical property of binder material itself, nor the adhesive strength between electrode film and current collector, but the cohesive strength between the polymeric binder and the Si particles that affects electrode performance the most.

2.2 Experimental

2.2.1 Electrode preparation and characterization

Si powder (size 30-50 nm, Nanostructured & Amorphous Materials) was used as the active material, Super C65 carbon black (denoted by CB, TIMCAL) as the conductive agent, PVDF (Alfa Aesar) and sodium alginate (denoted by SA, Sigma-Aldrich) as the binder. PVDF and SA were first dissolved in N-nethy-2-pyrrolidone (NMP, 99.5% Alfa Asear) and deionized water (denoted by DI water), respectively. A slurry was then prepared by mixing the active material, CB, and binder in a weight ratio of 2:1:1 using the Kurabo Mazerustar (KK-250S, Osaka, Japan) planetary mixer/deaerator. The Si/PVDF/CB and Si/SA/CB electrodes were made by casting the slurries using a doctor blade with an 80 μm gap size onto a copper foil. After drying at room temperature for 12 hours, the electrodes were transferred into a vacuum oven to further dry for another 12 hours at 110ºC. Scanning electron microscopy (SEM, FEI Quanta 250) observation was carried out to learn the microstructure of pristine electrodes, electrodes after the peel test, and electrodes after 200 electrochemical cycles, respectively. An optical microscope (Nikon, DXM-1200C) was also used to learn the structure of electrodes after performing the peel test.

2.2.2 Polymeric binder film preparation

A homogenous polymer PVDF/NMP (SA/DI) solution was obtained by mixing the solution in the planetary mixer/deaerator for 30 minutes. The PVDF/NMP (SA/DI) solution was then cast onto a Cu foil/silicon wafer (Wafer World) with a doctor blade. Finally, two

types of samples, polymer on copper foil (denoted by polymeric binder film@Cu foil) and polymer on silicon wafer (denoted by polymeric binder film@Si wafer), were dried with the same procedures mentioned in 2.2.1. Both films have similar smoothness and uniformity by visual inspection.

2.2.3 Peel test

Based on the ASTM D903 standard, several 180º peel tests have been carried out on an Instron 3345 tensile machine with a 10 N load cell. For peel tests of electrode films on Cu current collectors (denoted by electrode film@Cu foil) and polymeric binder film@Cu foil samples, a geometry shown in Fig. 2.1(a) was employed. Samples of 13 mm in width were pulled at a speed of 50 mm/min. For the polymeric binder film@Si wafer samples, the peel test geometry is shown in Fig. 2.1(b) without the aluminum plate and double sided tape shown in Fig. 2.1(a). A 13 mm wide strip of polymer binder film was obtained by using a knife to cut and remove the excess material. A piece of single sided tape was pulled by the upper grip at the same speed to test the adhesive strength between binder and silicon wafer.

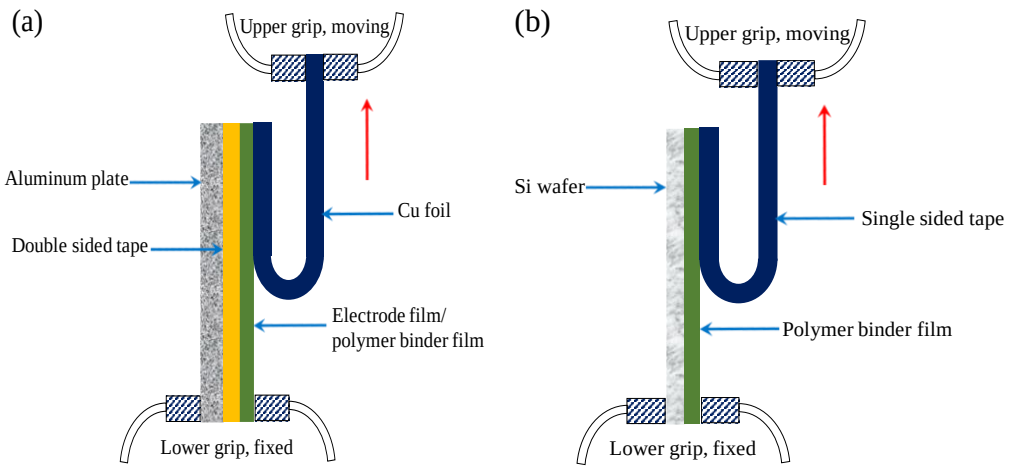

Figure 2.1 Geometries employed in peel tests. (a) geometry for the electrode film@Cu foil and polymeric binder film@Cu foil samples; (b) geometry for the polymeric binder film@Si wafer sample

2.2.4 Chemical analysis

Attenuated total reflection-Fourier transform infrared spectroscopy (ATR-FTIR, Nicolet iS10, Thermo Scientific) and x-ray photoelectron spectroscopy (K-Alpha XPS system, Thermo Scientific) were employed to investigate the possible chemical interactions between binder and Si in powder samples (PVDF+Si powder mixture and SA+Si powder mixture) and cast samples (PVDF+Si cast and SA+Si cast). The powder mixtures were prepared by mixing the Si particles and binder powders in a weight ratio of 2:1 in an alumina mortar. For cast samples, a slurry was first made by mixing the powders of Si and binder with solvents (NMP for PVDF and DI water for SA) in the same 2:1 weight ratio using the planetary mixer/deaerator and then cast onto a copper foil. After drying at room temperature for 12 hours, the samples were transferred into a vacuum oven to further dry for another 12 hours at 110ºC.

2.2.5 Electrochemical performance measurements

Electrochemical tests were performed in coin-type cells (CR2025) with Si electrodes as positive and a metallic lithium foil (Sigma-Aldrich) as both negative and

reference electrode. A microporous polyproplylene film (Celgard 3501) was used as a separator. 1M $LiPF_6$ salt in a 1:1 (wt/wt) mixture of ethylene carbonate (EC, BASF) and diethyl carbonate (DEC, BASF) with 10 wt% fluoroethylene carbonate (FEC, BASF) additive was used as an electrolyte. The cells were assembled in an argon-filled glove box (MBRAUN).

Cycling tests were carried out using a VMP3 potentiostats (Biologic) with a voltage window of 0.01 V-1 V versus Li/Li^+. The charging/discharging rate was set at C/10 for the first two cycles and C/3 for the rest of the cycles. A theoretical capacity of 3600 mAh/g was used to calculate the C rate.

2.3 Results and discussion

Peel tests were carried out on polymeric binder film@Cu foil and polymeric binder film@Si wafer samples to learn the adhesion behavior of polymeric binder on the Cu current collector and on silicon. At least three tests were performed with the two types of samples to assess the reproducibility of the measurement. Microstructure observations (Fig. 2.2-2.3) demonstrate that delamination occurred predominantly at the interface between polymeric film and Cu foil or Si wafer during the peel test.

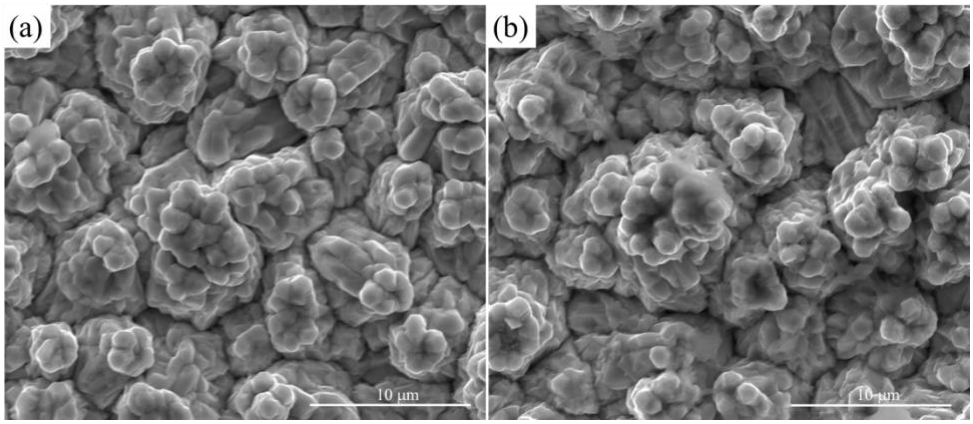

Figure 2.2 SEM images of polymeric binder film@Cu foil samples after peel test. (a) SA film@Cu foil sample; (b) PVDF film@Cu foil sample

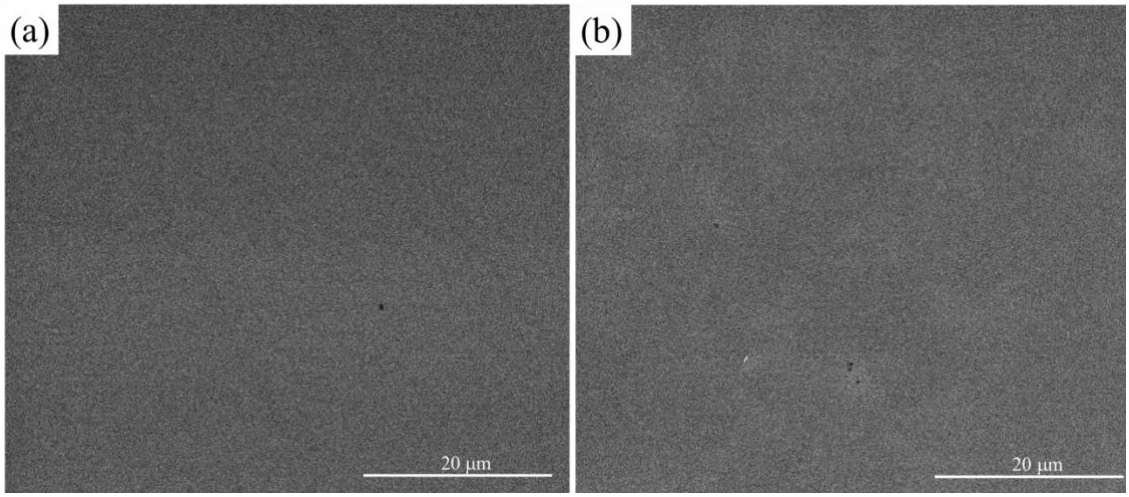

Figure 2.3 SEM images of polymeric binder film@Si wafer samples after peel test. (a) SA film@Si wafer sample; (b) PVDF film@Si wafer sample

Fig. 2.4(a) and 2.4(b) show the recorded peel strength-peel extension (S-E) curves for polymer film@Cu foil and polymer film@Si wafer, respectively. Here, the peel strength is defined as the force divided by the width of the sample and peel extension is the displacement of the upper grip. The median and standard deviation of the peel strength were calculated using the data with peel extension in the range of 2.5 mm-20 mm and the results are summarized in Table 2.1. In accordance with what has been predicted by a molecular dynamics study[130], the PVDF-Cu interface is quite strong to show a four times higher peel strength (91.3 N/m) than that of SA@Cu (20.5 N/m). SA@Si, on the other hand, has approximately three times higher adhesive strength (2.7 N/m) than that of PVDF@Si (1.0 N/m). Except for the interfacial strength between polymeric binder film and Cu current collector (Si wafer), the adhesion behavior of two types of Si composite electrodes were also examined and compared. As shown in Fig. 2.5, the Si/SA/CB electrode exhibits a peel strength of 78.3 N/m, which is about eight times higher than that of Si/PVDF/CB electrode (8.7 N/m).

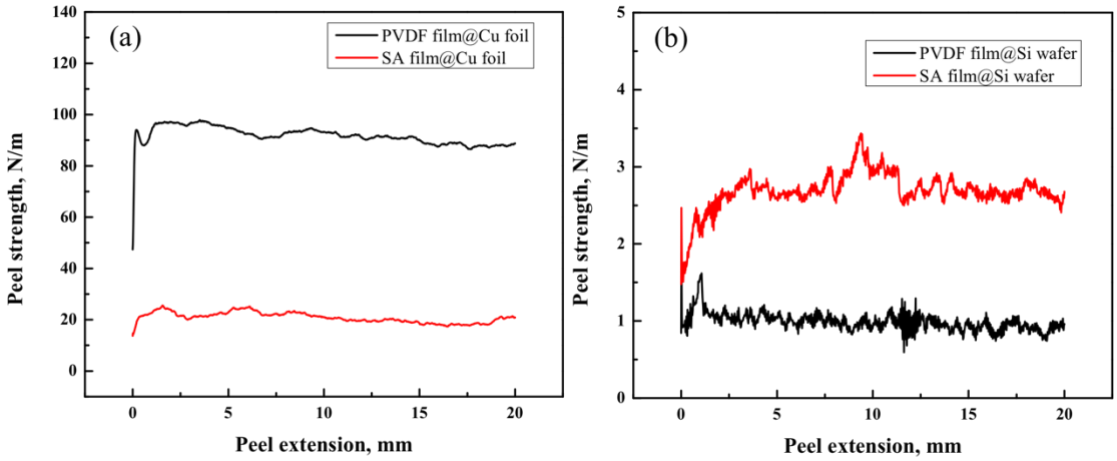

Figure 2.4 Peel strength-peel extension (S-E) curves of (a) polymeric binder film@Cu foil; (b) polymeric binder film@Si wafer

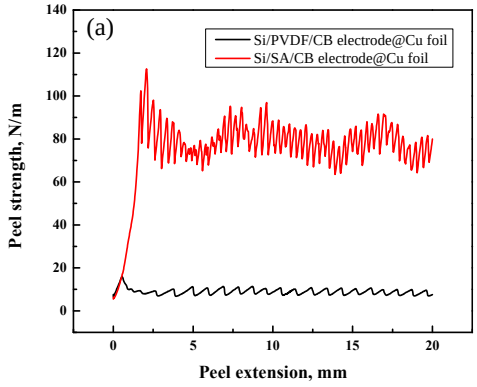

Figure 2.5 Peel strength-peel extension (S-E) curves of Si/SA/CB and Si/PVDF/CB electrodes

Table 2.1 Median peel strength of samples

	PVDF film@Cu foil	SA film@Cu foil	PVDF film@Si wafer	SA film@Si wafer	Si/PVDF/CB electrode@Cu foil	Si/SA/CB electrode@Cu foil
Peel strength (N/m)	91.3±2.8	20.5±1.9	1.0±0.1	2.7±0.2	8.7±1.1	78.3±6.6

In order to obtain a deeper understanding of the features in the S-E curves, scanning electron microscope was employed. As can be seen in Fig. 2.6(a)-(b), the surface of the electrodes after the peel test can be divided into two regions, one is bright and the other one is dark. SEM images with higher magnification, shown in Fig. 2.7, demonstrate that the dark region is covered by the electrode materials.

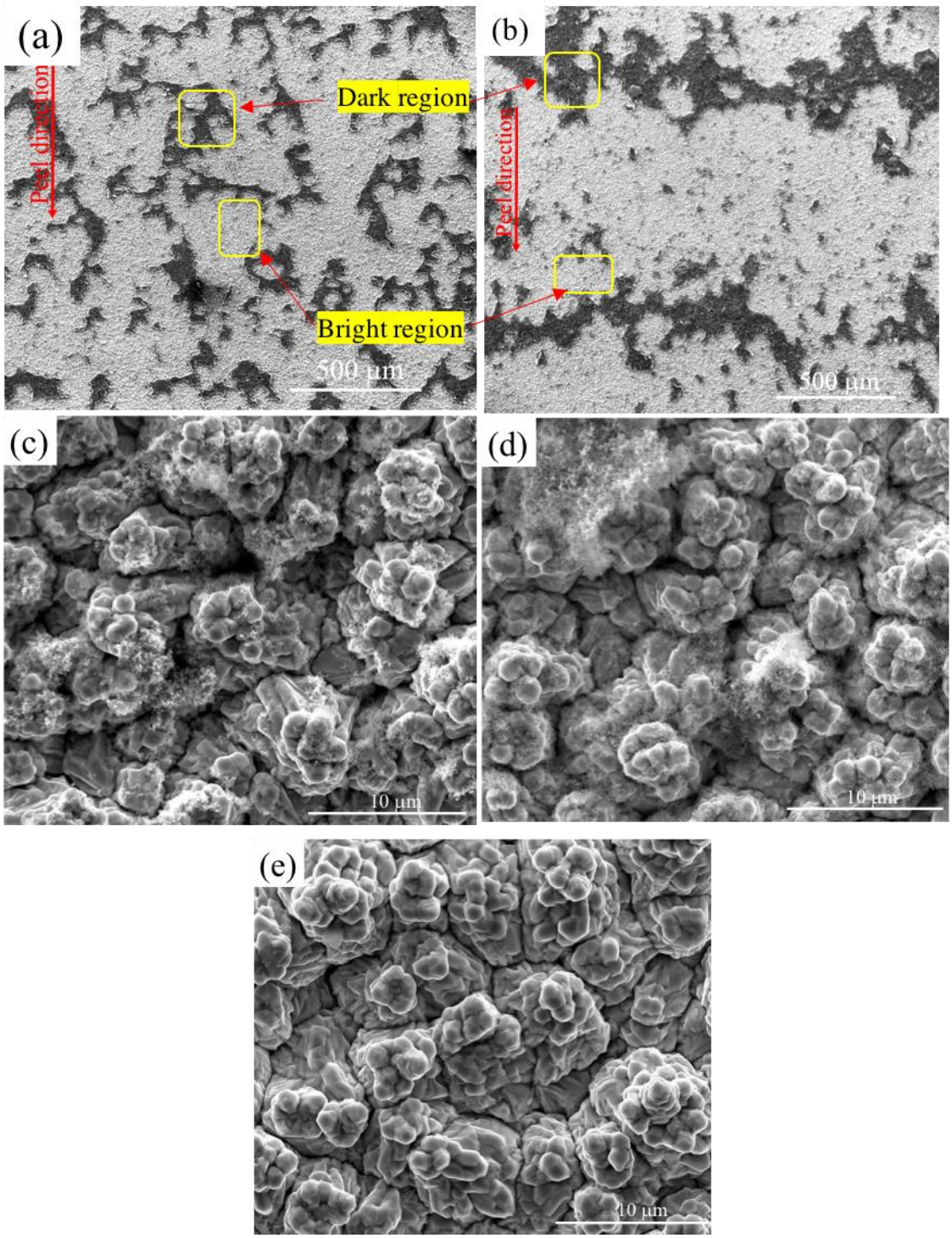

Figure 2.6 Microstructure of electrodes after peel test (a) Si/SA/CB electrode; (b) Si/PVDF/CB electrode; (c) Bright part in (a); (d) bright part in (b); (e) Surface of neat Cu foil

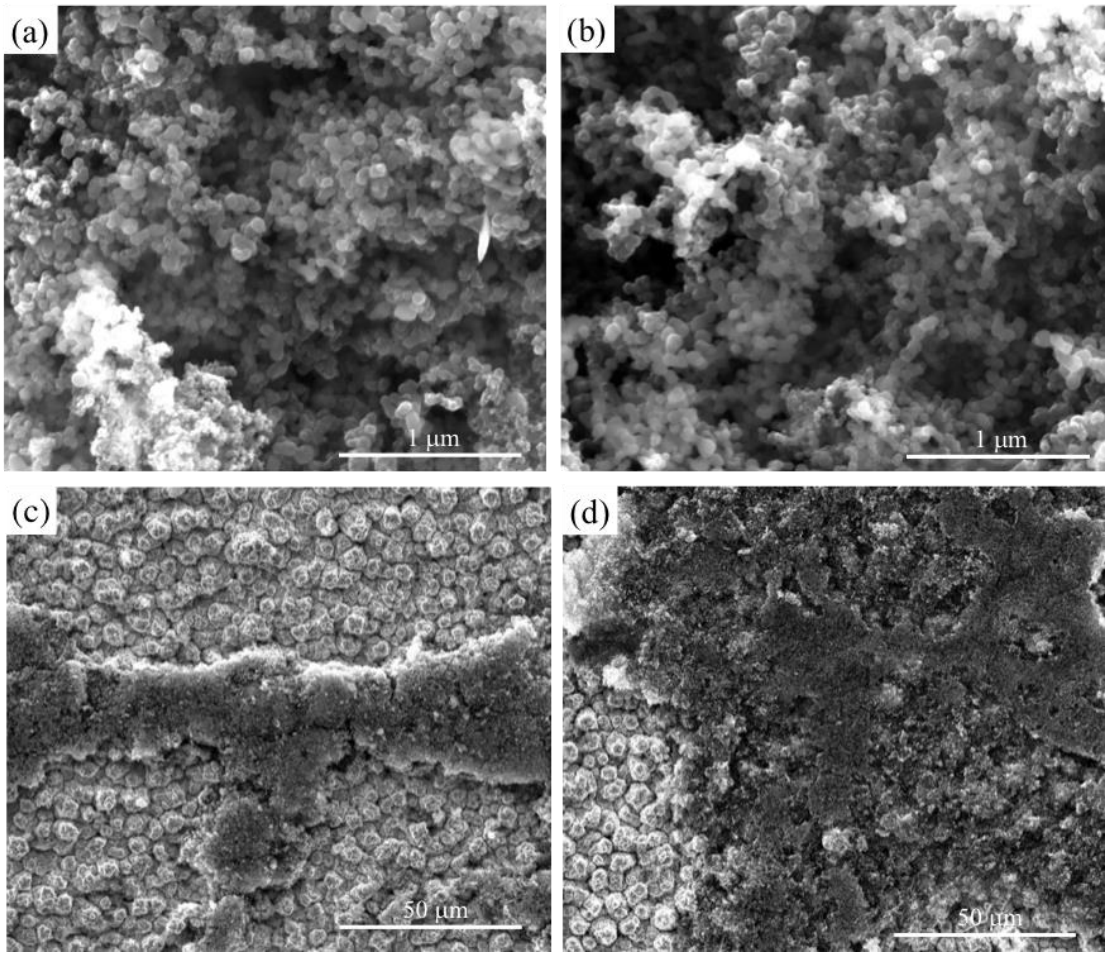

Figure 2.7 SEM images with higher magnification of the dark region (a)&(c) in Si/SA/CB electrode; (b)&(d) in Si/PVDF/CB electrode

Fig. 2.6(c) and 2.6(d) show the microstructure of the bright region in the Si/SA/CB and Si/PVDF/CB electrodes after peel test, respectively. Compared with the surface structure of the neat Cu foil shown in Fig. 2.6(e), much of the Cu surface is covered by abundant clusters consisting of a large number of electrode particles, especially for the Si/PVDF/CB sample. These observations suggest that the adhesion of both electrode to the Cu current collector is sufficiently strong to cause separation within the electrodes during the peel test. Since all of the dark region and most of the bright region are covered by electrode materials, the measured peel strength represents, predominately, the cohesive strength within the electrodes. Because of a stronger binder-silicon interface, Si/SA/CB

electrode has much higher cohesive strength than the Si/PVDF/CB electrode. It should be mentioned that sharp peaks and valleys were detected in the S-E curves of both electrodes (Fig. 2.8(a)), which are not random fluctuations and may be understood the following considerations. As the force increases, bright interface forms. At the same time, the curvature of the copper foil also increases until it reaches a maximum corresponding to the peak force on the S-E curve, causing an opening up of the interface within the electrode, generating a dark region in Fig. 2.6(a)-(b). When this newly formed interface propagates along the peel direction, curvature of the copper foil returns back to the initial value and the force decreases to the valley value. Then the force started to increase again to form another bright interface until it achieved next peak value followed by the formation of another dark interface. The whole peak-valley process repeated numbers of times periodically until the peel extension reached the ending point (20 mm in this paper). The sum of the width of one bright interface and one dark interface, as a result, is the distance between two peaks. From the enlarged S-E curves shown above in Fig. 2.8(a), it can be estimated that the distance between two peaks in Si/SA/CB and Si/PVDF/CB electrode is about 400 μm (distance between blue lines) and 1000 μm (distance between two green lines), respectively. Additional microstructure investigations from an optical microscope shown in Fig. 2.8(b)-(c) give similar results.

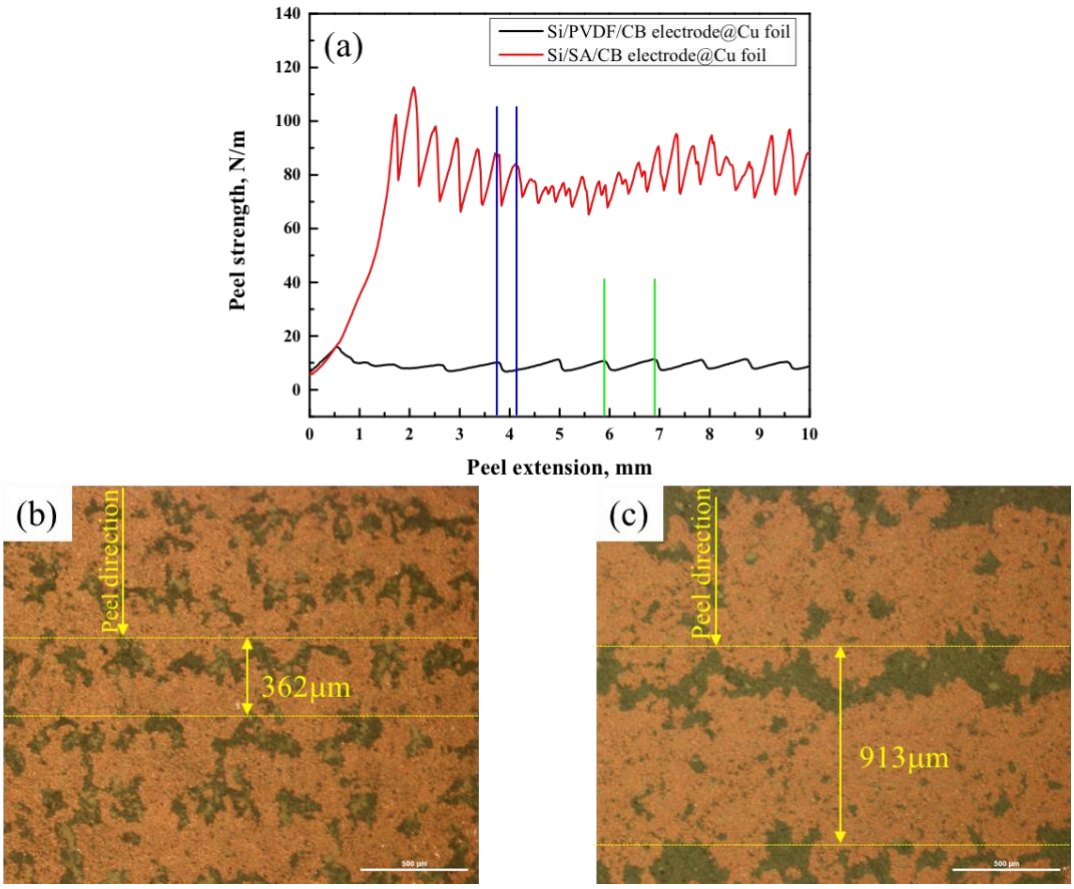

Figure 2.8 (a) Enlarged S-E curves of Si/SA/CB electrode and Si/PVDF/CB electrode; Optical microscopy image of silicon composite electrode after peel test (b) Si/SA/CB electrode; (c) Si/PVDF/CB electrode

The SEM observations shown in Fig.2.6-2.7 can also help understand why the peel strength of Si electrodes is much higher than the peel strength of pure polymeric films on silicon wafer (Fig. 2.4(b)). When a peel test was carried out in a polymeric film@Si wafer configuration, the separation occurred between polymer chains and a smooth and flat Si surface without the influence of any solid particles. In contrast, polymer bridging on multiple nearby Si particles would occur in an electrode, considering that the particle size of the Si powder used in the present work is quite small. As a result, a larger peel force is required to induce separation within the electrode.

Because the separation occurred predominately within the electrode during the

peel test, the adhesive strength between the Cu conductor and the electrode should be higher than the measured cohesive strength, i.e., the adhesive strength between the Cu conductor and the Si/SA/CB (Si/PVDF/CB) electrode is higher than 78.3 N/m (8.7 N/m). Comparing with the S-E curves shown in Fig. 2.4(a), it is evident that the adhesive strength in the Si/SA/CB (Si/PVDF/CB) electrode is significantly higher than that of the SA/Cu (PVDF/Cu) system. Similar to what has been discussed, polymer bridging between solid particles and the Cu current collector occurred during the electrode fabrication process, enhancing the adhesive strengths at the polymer-Cu interfaces and causing cohesive failures during the peel tests.

To determine the factors that influence the binder-Si interfacial strength, ATR-FTIR and XPS measurements were carried out. Fig. 2.9(a) shows the FTIR spectrum of bare silicon powders. The broad absorption peak at 3339 cm^{-1} is attributed to OH stretching vibration, the peaks at 2255 cm^{-1} and 2097 cm^{-1} correspond to $O_xSi–H$ and Si–H vibration[131, 132], the peak at 1627 cm^{-1} is ascribed to the O–H bending of adsorbed water, and the peaks at 1127 cm^{-1} and 875 cm^{-1} can be assigned to the stretching vibrations of Si–O–Si[133, 134]. For the pure PVDF (Fig. 2.9(b)), peaks located at 3024 cm^{-1} and 2983 cm^{-1} are assigned to asymmetric and symmetric vibration of CH_2[135], respectively. The peak at 1400 cm^{-1} is attributed to the in-plane bending of CH_2 group, the strong peak at 1179 cm^{-1} is mainly formed by the CF_2 symmetric stretching, the peak at 872 cm^{-1} represents out-of-plane deformation of CH group, and the peaks at 765 cm^{-1} and 614 cm^{-1} are related to CF_2 bending[136]. The absorption peaks in the FTIR spectra, shown in Fig. 2.9(c) and Fig. 2.9(d) for the respective PVDF+Si powder and PVDF+Si cast samples, can be assigned to the same peaks shown in pure Si particle or in pure PVDF. Since no new

peaks emerge in the PVDF+Si cast samples, covalent bonds did not form during the slurry making, casting, and drying process. The interaction between PVDF and Si is thus physical other than chemical, i.e., PVDF attaching to the surface of Si via weak van der Waals forces, which is consistent with another report[108].

The FTIR spectra of pure SA, SA+Si powder, and SA+Si cast samples are shown in Fig. 2.10. The SA powder spectrum, Fig. 2.10(b), exhibits a peak at 3233 cm^{-1} which can also be attributed to OH stretching vibration. The two peaks at 1594 cm^{-1} and 1409 cm^{-1} correspond to asymmetric and symmetric COO stretching vibration, and a peak at 1026 cm^{-1} is caused by C–O stretching vibrations, which agree with previous studies[111]. Fig. 2.10(c) and Fig. 2.10(d) show FTIR spectra of SA+Si powder and SA+Si cast sample, respectively. Similar to the PVDF+Si samples, the FTIR spectra of the SA+Si powder and the SA+Si cast sample do not show noticeable peak position changes. Thus, covalent bonds also did not form during the slurry making, casting, and drying process in the SA+Si sample.

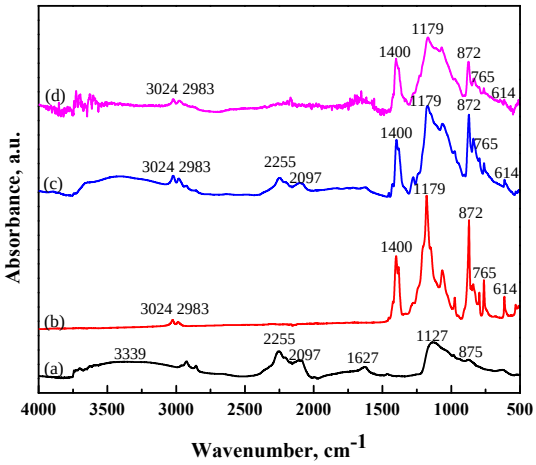

Figure 2.9 FTIR spectra of (a) Si powder; (b) PVDF powder; (c)PVDF+Si powder; (d) PVDF+Si cast

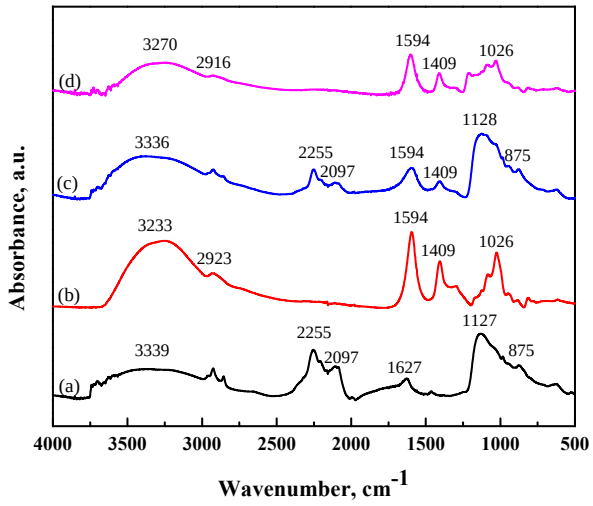

Figure 2.10 FTIR spectra of (a) Si powder; (b) SA powder;
(c) SA+Si powder; (d) SA+Si cast

XPS spectra of PVDF and SA containing samples are shown in Fig. 2.11(a) and Fig. 2.11(b), respectively. The C1s narrow scan of the PVDF+Si powder sample (Fig. 2.11(a)) display a peak that can be fitted by three peaks with binding energy at 291.17 eV for the CF_2 species, at 286.69 eV for CH_2 species, and at 284.85 eV for the neutral C-C species. The ratio for the CF_2 and CH_2 peaks is about 1:1, in agreement with the chemical structure of PVDF[137]. Fig. 2.11(b) shows C1s spectra of the SA+Si powder sample and SA+Si cast sample, which require four peaks to fit. The peaks located at 284.77, 286.31, 288.17, and 289.58 eV can be assigned to C-C, C-O, O-C-O, and COOH bonds, respectively.

Similar to what is observed from the FTIR results, all XPS peaks in the physical mixture of binder and Si exist in both PVDF and SA containing cast samples with no new peaks emerged. Thus, both FTIR and XPS show that covalent bonds do not form between the two binders and Si particles during the electrode fabrication process.

Although no covalent bond formed between SA and Si, other types of chemical bonds may emerge considering the surface chemistry of Si and chemical structure of SA.

Transmission electron microscopy (TEM) demonstrates that there is an oxide layer of a few nanometers thick on top of the Si particle (Fig. 2.12). Strong hydrogen bonding between the hydroxylated Si surface and –COOH, –OH, and –O– groups in SA could form, which has been previously identified as one of the most critical factors affecting the stability of Si-based electrodes[127], resulting in a stronger interface between SA and Si particles.

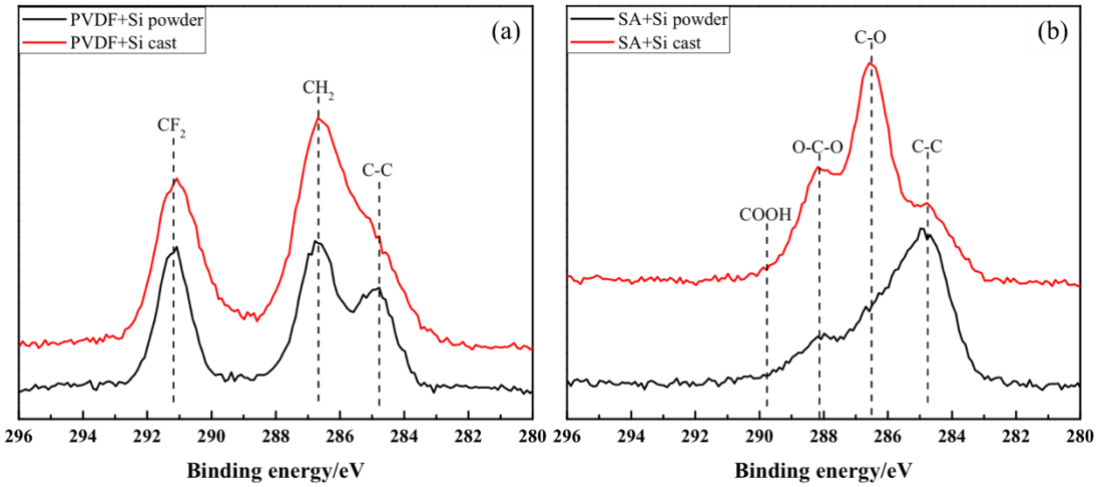

Figure 0.11 XPS C1s spectra of (a) PVDF+Si samples; (b) SA+Si samples

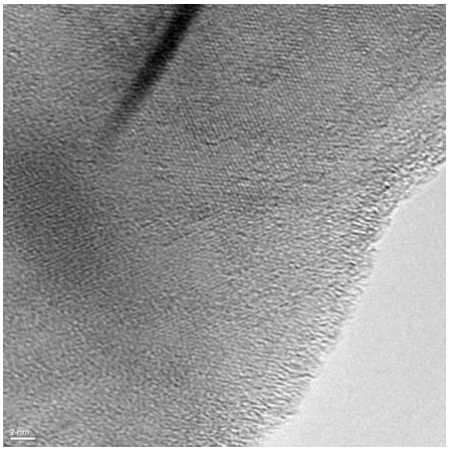

Figure 2.12 TEM image of Si particle

Fig. 2.13(a) shows the electrochemical cycling performance of the two types of Si electrodes. The Si/PVDF/CB electrode fades quickly with approximately 350 mAh/g

discharge capacity delivered after 200 cycles. In contrast, the Si/SA/CB electrode shows much better cycling performance, maintaining its discharge capacity over 2800 mAh/g for 200 cycles under the same test condition. Consistent with previous observations[108, 126, 138-142], the discharge capacity first increases for about 25 cycles and then decreases with increasing cycle number for the Si/SA/CB electrode, which may be understood by the following limited capacity cycling measurements.

In Fig. 2.13(b), the Si/SA/CB electrode cycles stably at a rate of C/3 with a lithiation capacity limit of 900 mAh/g for over 600 cycles. In contrast, the Si/PVDF/CB electrode cannot deliver the same capacity after 20 cycles. Its lithiation cut-off potential also decreases quickly as depicted in Fig. 2.13(c). One factor that contributes to the poor performance is the weak binder-active particle interface. Because of the low PVDF-Si interfacial strength, Si particles can detach from the polymer chains upon volume expansion/contraction during electrochemical cycling. These Si particles become electronically isolated and can no longer participate in the electrochemical reaction. The remaining Si particles have to take more lithium to achieve the designated capacity, leading to higher Li to Si ratio and, accordingly, a lower potential of the electrode. With further cycling, more and more particles detach from the electrode and the targeted capacity cannot be achieved.

In the Si/SA/CB electrode, the cut-off potential increases from about 0.07 V to about 0.11 V in the first 20 cycles, then stabilizes at 0.11 V for more than 600 cycles as seen in Fig. 2.13(c). Comparing Fig. 2.13(c) with Fig. 2.13(a), we notice that the initial increasing potential stage in Fig. 2.13(c) corresponds to the stage of increasing discharge capacity shown Fig. 2.13(a). This correlation suggests that some of the Si particles may be

too well covered by the SA polymer which is an electronic and ionic insulator and, as a result, these Si particles initially do not fully participate in lithiation and delithiation. The volume expansion/contraction of the active Si particles can induce the deformation and movement of surrounding polymeric binders, enabling the well-covered Si particles to contact the electrolyte and become electrochemically active. Thus, with more and more Si particles participating in the electrochemical reaction, the discharge capacity increases with increasing cycle number as shown in Fig. 2.13(a). For the limited lithiation capacity experiment shown in Fig. 2.13(b), the active Si particles have to take more Li to reach the lithiation limit because of the well-covered Si particle are electrochemically inactive initially. Consequently, these Si particles have a higher Li to Si ratio, leading to a lower cut-off voltage. As the inactive Si particles become active during the first 20 expansion/contraction cycles, more Si particles participate in lithiation/delithiation, resulting in a lower Li:Si ratio and an increase in the cut-off voltage. After about 20 cycles, a steady amount of the Si particles become active, the cut-off potential of the Si/SA/CB electrode stabilizes at 0.11 V. Because active particles are held together by the SA polymer chains tightly, the tendency for Si particles to detach from the electrode is reduced in the Si/SA/CB electrode, enabling an excellent cycle life in the Si/SA/CB electrode under the capacity limit cycling conditions.

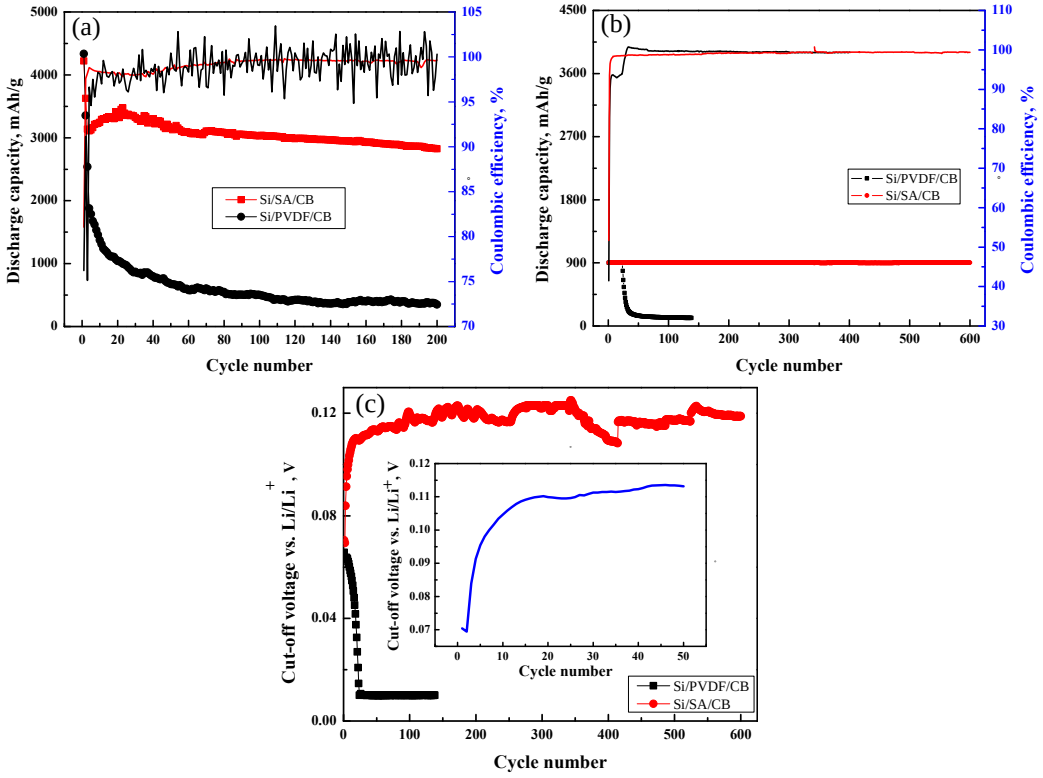

Figure 2.13 Electrochemical performance of Si/SA/CB and Si/PVDF/CB electrodes (a) C/10 for the first two cycles and C/3 for rest of the cycles (b) C/3 for all cycles with capacity limit of 900 mAh/g (c) cut-off voltage of the electrodes tested with capacity limit

2.4 Conclusion

Peel strength has been measured and correlated with both electrochemical performance and microstructure of Si composite electrodes. The cohesive strength in the Si/SA/CB electrode and the Si/PVDF/CB electrode has been found to be 78.3 N/m and 8.7 N/m, respectively. It was demonstrated that to have a strong polymeric binder-active particle interface is decisive in ensuring a good cycling performance and long cycle life. Mechanical property of binder and adhesive strength of electrode to the current collector are not necessarily key parameters. No covalent bond formed between binder and Si particles during the slurry making, casting, and drying process. The stronger SA-Si interface is attributed to hydrogen bonding that could form between the hydroxylated Si

surface and –COOH, –OH, and –O– groups in SA. The present work may provide a guide and an approach for design and optimization of binder materials in Si composite electrodes.

Chapter 3 Oxidative pyrolysis of Si/polyacrylonitrile composites as an unconventional approach to fabricate high performance lithium ion battery negative electrodes

3.1 Introduction

Si has been extensively studied as one of the most promising negative electrode materials for the next generation lithium ion batteries (LIBs), because it possesses a high theoretical capacity of 3579 mAh/g ($Li_{15}Si_4$) - almost ten times higher than that of graphite (372 mAh/g), the most commonly used negative electrode material in commercial LIBs. However, accompanied with the high theoretical capacity is the ~300% volume expansion upon its fully lithiation, which can cause pulverization of particles, delamination of the electrode layer from the current conductor, continuous growth of the solid electrolyte interphase (SEI), and breakdown of electronic/ionic transport paths, resulting in low coulombic efficiency and rapid capacity fade of the Si-based electrodes.

To mitigate the detrimental effects of the large volume expansion, several strategies, such as applying functional polymer binders[105, 108, 110], developing novel nano-Si architectures[44, 47, 51], and surface coating[60, 143, 144], have been investigated. Of these strategies, Si-C composite electrodes are especially promising, because carbon is relatively inexpensive, flexible, and electronically conducting. Various methods, e.g., carbonization of precursors[85, 115, 145-147], sputtering[113, 148], filling the pores of porous Si with carbon[149], pyrolysis of polymer[150], ball milling of Si with carbon[151, 152], and electrospinning followed by carbonization[153-156], have been employed to synthesize Si-C composite electrodes. Although the performance of Si-C composite electrodes is superior to that of bare Si electrodes, some of the aforementioned methods involve multiple time-consuming and complicated processing steps which make

the large-scale commercialization of these methods difficult. More importantly, Piper et al.[157] pointed out that the volume expansion could not be effectively accommodated by the carbon in these Si-C composites because of their tendency for brittle failure. Instead, they showed that Si/PAN composite electrodes exhibited promising electrochemical performance if the pyrolysis temperature was limited to 300-500^{o}C, during which the PAN became cyclized instead of being fully carbonized. Similar observations have also been reported by Tersak et al.[158] and Thakur et al.[62]. These studies suggest that cyclization of PAN occurs when it is treated in an inert environment at a relatively low temperature, and the cyclized PAN can function as both the binder and conductive matrix to assure a superior electrode performance.

Researchers from the carbon fiber community have known that the cyclization/stabilization of PAN can be accomplished by pyrolysis of PAN either in an inert or a reactive atmosphere at a temperature up to 400^{o}C[159-162]. In fact, Bahl et al.[163] showed that, compared with the PAN treated in an inert environment, the presence of oxygen in air facilitated the cross-linking of PAN. However, heat treatment of Si/PAN composites in the presence of oxygen, namely the oxidative pyrolysis of Si/PAN composites, to the best of our knowledge, has not been reported in the LIB literature.

Extensive reactions of PAN with oxygen could form volatile products such as CO and CO_2, leading to issues, such as poor electrode integrity, bad adhesion between electrode layer and the current collector, and inferior electrochemical performance. In this work, we attempt to answer the following questions: Can we control the oxidative pyrolysis conditions such that PAN does not completely burn out from the Si/PAN composites? Can oxidative pyrolysis produce Si/PAN composites with both high electronic conductivity and

mechanical flexibility? Can the Si/PAN electrodes have similar or better electrochemical cycling performance than that made through pyrolysis in the inert environment?

3.2 Experimental

3.2.1 Preparation of Si/PAN composite electrodes by oxidative pyrolysis

Si powder (size 150 nm, Paraclete Energy) and PAN (Mw 150,000, Sigma-Aldrich) were the active material and binder, respectively. The PAN solution was prepared by dissolving PAN in N-nethy-2-pyrrolidone (NMP, 99.5%, Alfa Asear). Electrode slurries were then made by mixing Si powder in the PAN solution to achieve a Si:PAN weight ratio of 3:2 in a planetary mixer/deaerator (Mazerustar KK-250S, Kurabo). Si/PAN composite electrodes (fresh electrodes) were prepared by casting the slurries onto a copper foil followed by a drying process which was carried out at 80ºC for 12 hours in a convection oven (Yamato, DKN 812). They were then sent to a furnace (Type 30400, Thermolyne) and held at 250, 300, 350, or 400$_o$C for 30 minutes in air to complete the oxidative pyrolysis.

3.2.2 Coin cell fabrication and electrochemical measurements

Electrochemical measurements were performed in coin-type cells (CR2025) with Si/PAN electrodes as the positive and a metallic lithium foil (Sigma-Aldrich) as both the negative and reference electrode. The average mass loading of Si in the Si/PAN composite electrodes was 1 mg/cm$_2$. A microporous polyproplylene film (Celgard 3501) was used as the separator. The 1M LiPF$_6$ dissolved in a 1:1 (w/w) mixture of ethylene carbonate (EC, Gotion) and diethyl carbonate (DEC, Gotion) with 10 wt.% fluoroethylene carbonate (FEC, Gotion) was used as the electrolyte. The cells were assembled in an argon-filled glove box (MBRAUN).

Cycling tests were carried out using a VMP3 potentiostat (Biologic) with a voltage window of 0.01 to 1.00 V versus Li/Li^+. The charging/discharging rate was set at C/10 (0.36 A/g) for the first two cycles and C/3 (1.2 A/g) for the subsequent cycles. A theoretical capacity of 3600 mAh/g was used to calculate the C rate. The electrochemical impedance spectroscopy (EIS) was performed using the same equipment at fully delithiated state and an AC oscillation amplitude of 5 mV at a frequency range of 0.01Hz-100 kHz. Cyclic voltammetry (CV) results of Si/PAN composite electrodes were also obtained using the same instrument over a voltage window of 1.2 V to 0.01 V at a scanning rate of 0.1 mV/s.

3.2.3 Materials Characterization

Thermogravimetric analysis (TGA) was conducted on Q5000 SA (TA Instruments) where PAN was heated from 25 to 600^{o}C in air at a heating rate of 10^{o}C/min. Scanning electron microscopy (SEM) and energy dispersive X-ray spectroscopy (EDS) were performed with FEI Quanta 250. Raman spectroscopy measurements were carried out with a DXR^{TM}2xi Raman Imaging Microscope (Thermo Scientific). X-ray photoelectron spectroscopy (XPS) was carried out on a K-Alpha XPS system (Thermo Scientific). A Siemens D5000 X-ray diffractometer was employed to identify the possible phase change of Si/PAN composites after heat treatment. A Talos transmission electron microscope (TEM, Thermo Scientific) was used to observe the microstructure of the Si/PAN composites. A Hitachi IM4000plus ion milling system was used to cut the Si/PAN composites for observing the cross-sectional microstructures.

3.2.4 Mechanical property measurements

The mechanical properties of Si/PAN composites before and after heat treatment were investigated by nanoindentation using a Nanoindenter (G200, Agilent Technologies). A diamond Berkovich indenter tip was employed to make ten indents on each sample at random locations. A depth-controlled mode was used to carry out the indentation tests with the following procedures: indenting each sample at a constant strain rate of 0.05 1/s to the depth limit, holding the indenter at the maximum load for 10 seconds, then unloading the indenter at a constant rate (-0.12 mN/s). To avoid any influence from the copper current collector substrate, the indentation depth was limited to 10% of the total thickness of the electrode layer (the electrode thickness is 11 μm in this work).

3.3 Results and discussion

The electrochemical behaviors of Si/PAN composite electrodes are presented in Fig. 3.1. As shown in Fig. 3.1(a), the 250^{o}C treated sample displays the worst performance with its discharge capacity dropping to 630 mAh/g at the 10th cycle and nearly zero after 60 cycles. After increasing the temperature to 300^{o}C, the discharge capacity is 1415 mAh/g at the 10th cycle and retains 1132 mAh/g at the 100th cycle, a considerable improvement over the electrode prepared at 250^{o}C. Even better performance is observed after increasing the temperature further. The discharge capacity of the 400^{o}C treated Si/PAN composite electrode is higher than 2000 mAh/g for more than 60 cycles and is 1614 mAh/g at the 100th cycle. Fig. 3.1(b) displays the 1st discharge/charge curves of the Si/PAN composite electrodes. Similar to those reported in the literature [108, 111], all electrodes show a long plateau with potential <0.1V, which corresponds to the amorphization of Si. Intriguingly, both the 350^{o}C and 400^{o}C treated Si/PAN composite electrodes deliver a first lithiation

capacity of 4500 mAh/g which is larger than the theoretical capacity of 4200 mAh/g for the $Li_{22}Si_5$ phase. The CV curves in Fig. 3.2 (a) show that a lithiation peak at about 1.1 V appeared in the 350°C and 400°C treated Si/PAN composite electrodes in the first cycle. This may be the result of side reactions between Li and the pyrolyzed PAN in the Si/PAN composite after the heat treatment since carbon onions, which have lithiation capacity [164-166], are detected in the 400°C treated Si/PAN composite (Fig. 3.12).

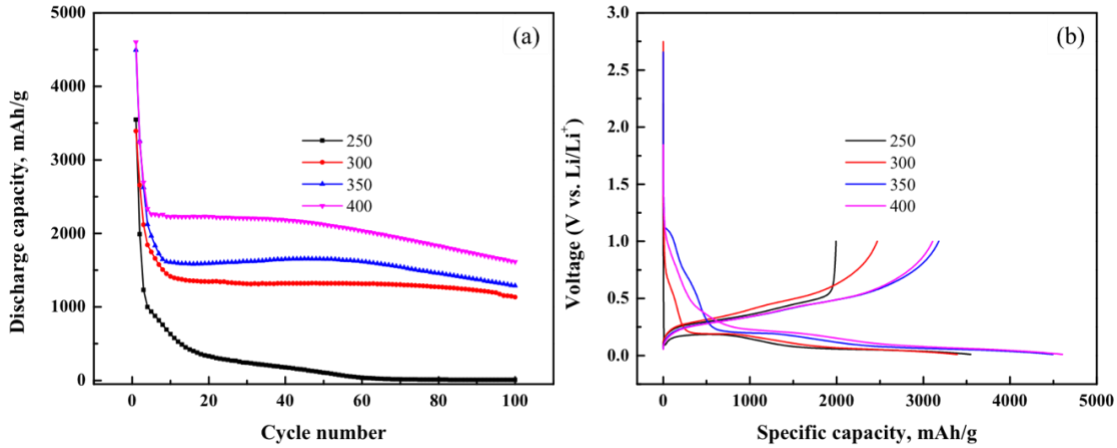

Figure 3.1 Electrochemical performance of Si/PAN composite electrodes: (a) long term cycling with C/10 for the first two cycles and C/3 for the subsequent cycles; (b) first discharge/charge voltage profile cycled at C/10. The numbers 250, 300, 350, and 400 in the figure represent the heat treatment temperatures of 250°C, 300°C, 350°C, and 400°C

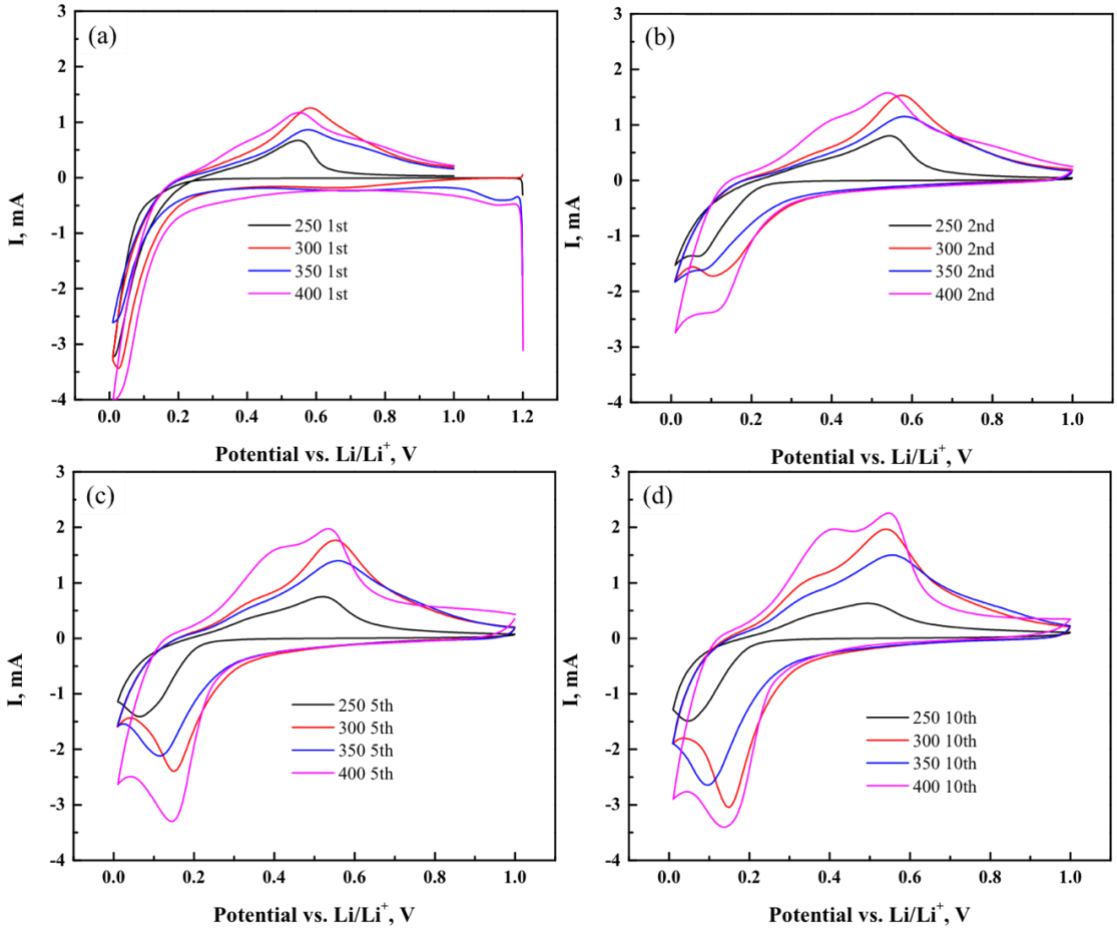

Figure 3.2 Cyclic voltammograms of Si/PAN composite electrodes (a) first cycles, (b) second cycle, (c) 5th cycle, (d) 10th cycle

Si/PAN composites treated at elevated temperatures also exhibit increased rate capability as seen in Fig. 3.3. The 250ₒC treated composite electrode shows the poorest performance among the electrodes tested, while the 400ₒC treated Si/PAN composite electrode appears to be the best. When cycled at 3C, the 400ₒC treated sample delivers an impressive discharge capacity of about 500 mAh/g, while others show almost zero capacity. Moreover, it has a capacity of nearly 3000 mAh/g when the C rate is returned to C/10, revealing that the electrode is able to return to its original capacity after multiple lithiation/delithiation cycles at high current rates. EIS spectra (Fig. 3.4), together with the fitting data (Table 3.1) demonstrate that the 400ₒC treated Si/PAN composite has the most

stable SEI and the lowest charge transfer resistance at all cycles, indicating both good Li alloying and de-alloying kinetics and high electronic conductivity.

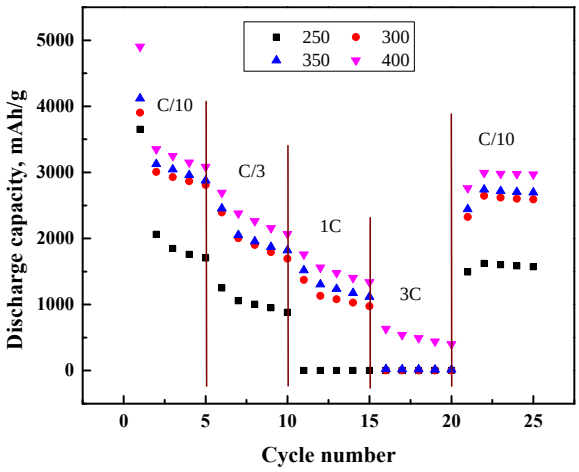

Figure 3.3 Rate performance of Si/PAN composite electrodes

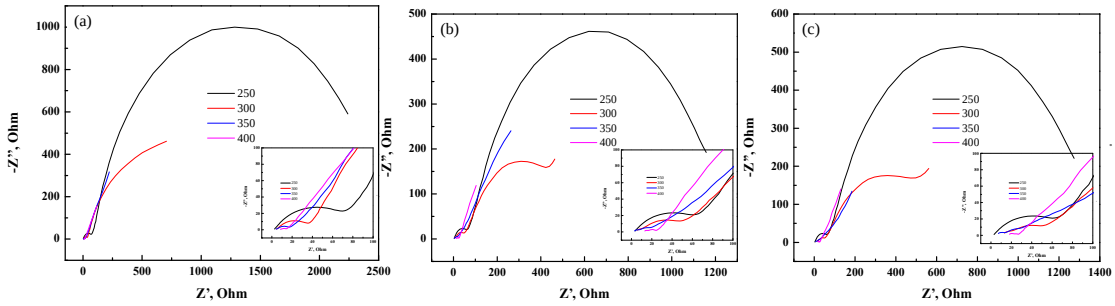

Figure 3.4 EIS spectra of Si/PAN composite electrodes (a) after two cycles, (b) after 50 cycles, (c) after 100 cycles. Detailed EIS spectra at high frequency are shown in the inserted

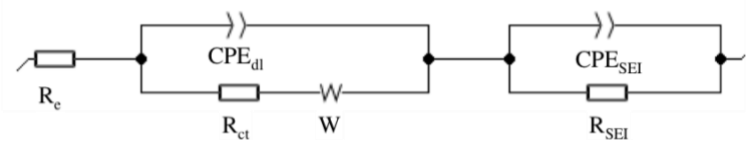

Figure 3.5 Equivalent circuit used to fit the EIS spectra shown in Fig. 3.4

Table 3.1 R_{SEI} and Rct of Si/PAN composite electrodes

	After 2 cycles		After 50 cycles		After 100 cycles	
	R_{SEI} (Ω)	R_{ct} (Ω)	R_{SEI} (Ω)	R_{ct} (Ω)	R_{SEI} (Ω)	R_{ct} (Ω)
250	80.0	2497.0	69.1	1185.0	69.4	1341.0
300	33.9	951.7	50.9	470.8	44.2	580.4
350	3.0	8.8	3.7	13.8	5.6	21.6
400	2.2	3.2	4.9	6.6	6.5	2.8

To help understand the effect of oxidative pyrolysis on the microstructure and thus the electrochemical performance of Si/PAN composites, XRD patterns, SEM observations, and EDS elemental mapping results are compared. Shown in Fig. 3.6 are the XRD patterns of Si/PAN composites before and after oxidative pyrolysis. All diffraction peaks can be assigned to either Si or the Cu current collector, except that a portion of Cu is oxidized in air and converted to Cu_2O if the processing temperature is higher than 350^{o}C. Fig. 3.7 is the cross-sectional SEM images of the Si/PAN composites. The surface microstructures of the same samples can be found in Fig. 3.8. Evidently, the 250^{o}C treated Si/PAN composite has a microstructure similar to that of the fresh sample; the space between Si particles is nearly fully occupied by the polymer. Above 300^{o}C, the Si/PAN composites become increasingly porous with increasing temperature. The pores can provide room for the expansion/contraction of Si particles. The electrolyte can infiltrate the pores to enhance the electrochemical performance, especially at high C-rates.

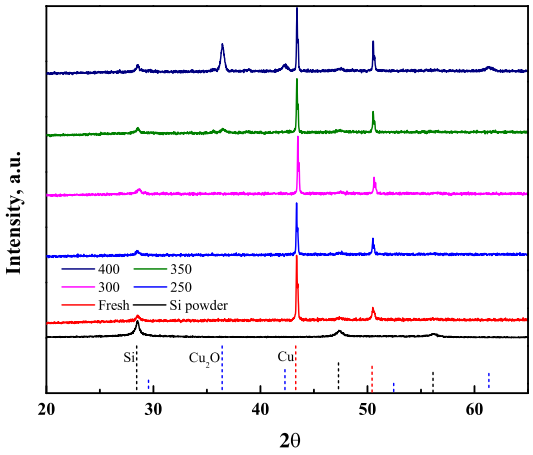

Figure 3.6 XRD patterns of Si/PAN composite electrodes

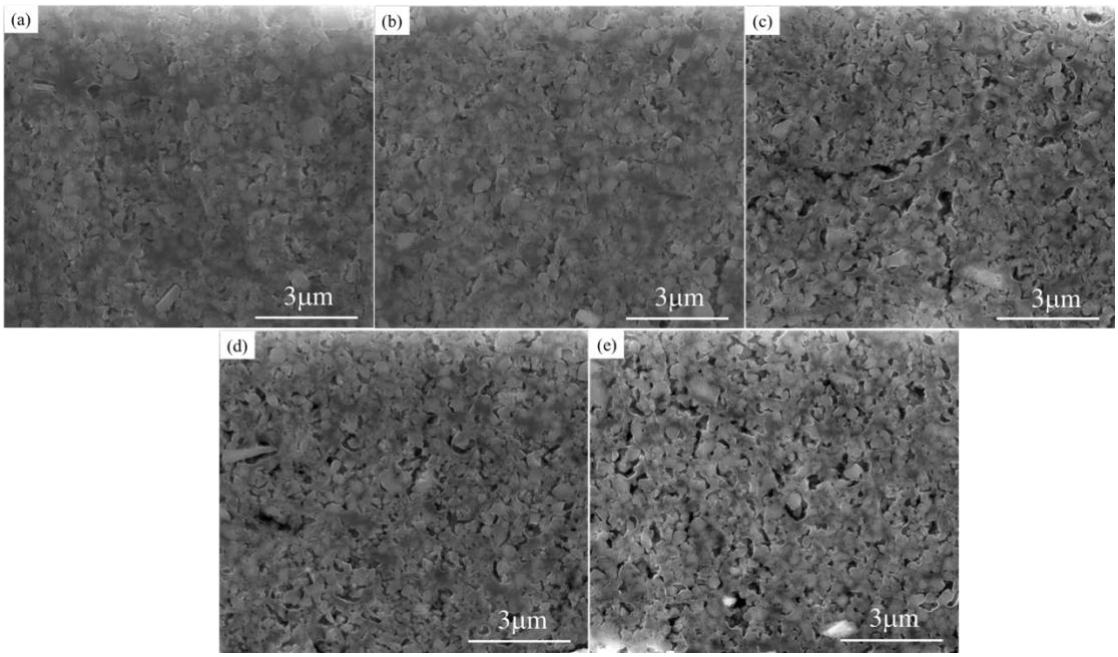

Figure 3.7 Cross sectional SEM images of Si/PAN composite electrodes: (a) fresh, (b) treated at 250ºC, (c) treated at 300ºC, (d) treated at 350ºC, and (e) treated at 400ºC

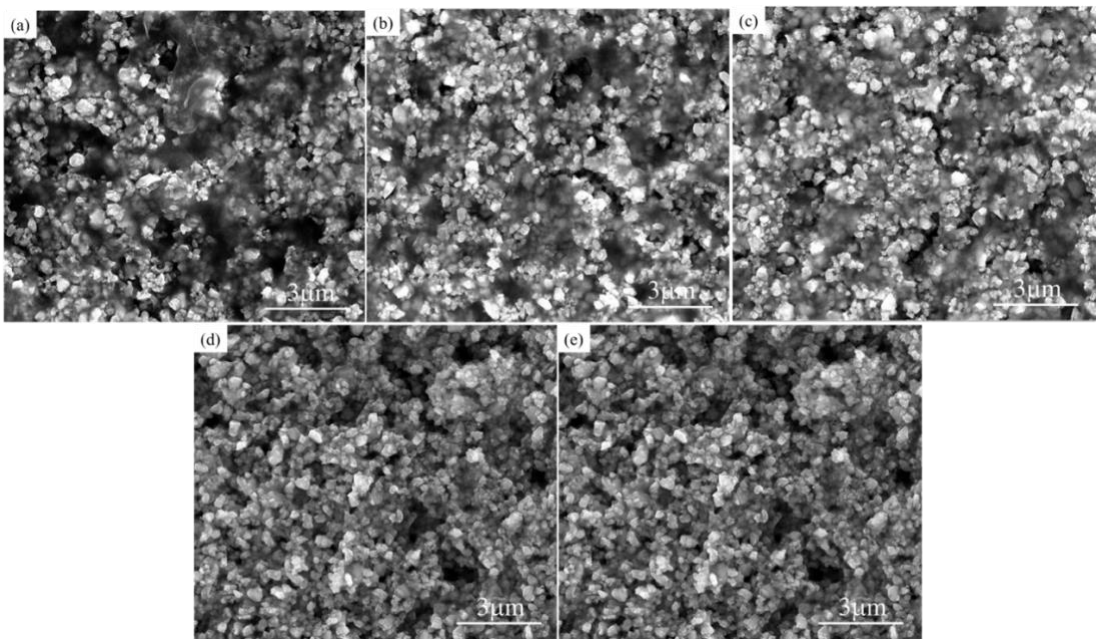

Figure 3.8 Surface microstructures of Si/PAN composite electrodes: (a) fresh, (b) treated at 250$_o$C, (c) treated at 300$_o$C, (d) treated at 350$_o$C, and (e) treated at 400$_o$C

Table 1 summarizes the chemical compositions (obtained from the EDS mapping) of the Si/PAN composites. Compared with the fresh Si/PAN composite, similar amounts of Si, C, and N but increased O is detected in the 250$_o$C treated sample. Since the extensive oxidation of Si at a temperature lower than 400$_o$C is limited[167], the increased O concentration is most likely caused by the O incorporated in PAN to form N-oxide bonds, whose presence is further confirmed by the XPS results discussed in more detail later in the paper. At temperatures exceeding 300$_o$C, more Si and O but less C is detected. The decreasing C concentration may be caused by the burning out of PAN from the Si/PAN composites. The TGA curve of PAN (Fig. 3.9) shows that the mass loss of PAN starts at 300$_o$C and becomes more severe with increasing temperature. Consequently, a decreasing C concentration in the Si/PAN composites is observed.

Table 3.2 Compositions of Si/PAN composite electrodes

	Si (wt%)	C (wt%)	N (wt%)	O (wt%)
Fresh	55.3±0.3	35.6±0.3	5.3±0.2	3.8±0.1
250	55.3±0.3	34.3±0.3	5.8±0.2	4.6±0.1
300	57.0±0.3	29.5±0.3	6.0±0.3	7.4±0.1
350	58.1±0.3	28.7±0.3	5.5±0.3	7.6±0.1
400	60.5±0.3	26.7±0.3	5.2±0.3	7.6±0.1

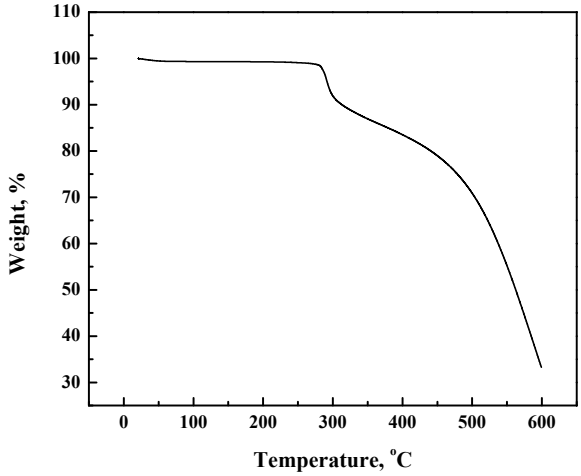

Figure 3.9 TGA curve of PAN

In general, structural studies show that a growing amount of PAN and/or the products from the oxidization of PAN leave the Si/PAN composites with increasing temperature, producing a progressively porous structure with increasing concentration of Si in the composites. It needs to be mentioned that oxidative pyrolysis at even higher temperatures, e.g., 450$_o$C and 500$_o$C were also explored in this work. However, we found that further increase the temperature induces over burn of PAN, resulting in poor mechanical integrity, weak adhesion, and interior electrochemical performance of the Si/PAN composite electrode.

To investigate the relationship between the chemical bonding and electrochemical performance of Si/PAN composites, XPS and Raman spectroscopy were performed. The results are shown in Fig. 3.10 and Fig. 3.11, respectively. Shown in Fig. 3(a) are the high-resolution C1s spectra of Si/PAN composites. Two peaks located at 284.8 eV (C-C) and 286.2 eV (C≡N) are observed in the composites before the oxidative pyrolysis. A new peak that represents C-O or C-N (286.6 eV) appears when the Si/PAN composite is treated at 250$_o$C, as shown in Fig. 3.10 (b). For the composites treated above 300$_o$C, the peak at 286.2 eV vanishes while the peaks at 288.9-298.2 eV (C=OO), 286.6 eV (C-O, C-N), and 284.8 (C-C) remain. Fig. 3.10 (c) is the N1s XPS spectra of the Si/PAN composites before and after oxidative pyrolysis. Similar to what has been discussed with the C1s spectra, only one peak at 399.1 eV is observed in the N1s XPS spectra (Fig. 3.10(c)) of fresh samples, which is attributed to the C≡N functional group. After the heat treatment at 250$_o$C for 30 minutes, two new peaks located at 398.6 eV (pyridinic) and 400.1 eV (pyrrolic) appear. Cyclization of PAN in the oxidizing atmosphere, which is normally believed to initiate at around 180$_o$C [168], occurs in a small portion of the polymer, causing the structural change. The cyclization process of PAN is believed to involve oligomerization of nitrile groups during which C≡N triple bonds convert to C=N double bonds with the N atom in the original nitrile group forming a C−N single bond with another carbon[169], resulting in a ring structure. With increasing temperature, chemical reactions, e.g., dehydrogenation and oxidation, along with more cyclization, occur to form the stabilized PAN. It has been reported by Gupta et al.[170]. and Mittal et al.[171] that stabilization of PAN could be completed at a temperature around 300$_o$C. Consistent with the literature, we found that the signal from nitrile groups disappears from the N1s spectra when the temperature is higher

than 300^{o}C. Alternatively, three peaks representing pyrrolic (400.0-400.1 eV), pyridininc (398.5-398.6 eV), and N-oxide (402.9-403.3 eV) groups are detected, indicating that the original linear PAN chains are absent, but all stabilized PAN molecules remain in the Si/PAN composites. However, the stabilization of PAN is very complicated with several proposed reaction mechanisms and different structures[172].

The ratio of various N-containing sites in each sample is compared in Table 3.2. With increasing temperature, there are fewer pyridinic but more pyrrolic groups left in the Si/PAN composites. The N atom in the pyridinic group is generally believed to form sp^2 hybridized bonds with two C atoms and enable good electrical conductivity. In contrast, the N atom is sp^3 hybridized in a five-membered ring in the pyrrolic group, which is insulating[173]. Therefore, one would expect the Si/PAN composite with the most pyridinic-N (300^{o}C treated sample) to have the highest electronic conductivity and perhaps the best performance. The 300^{o}C treated sample does show much improved electrochemical performance compared with the 250^{o}C treated sample, but is not as good as the samples treated at 350 and 400^{o}C. It has been suggested that additional aromatization and intermolecular crosslinking can happen when PAN is stabilized at a temperature up to 400^{o}C[171, 174-176], which may be beneficial to establishing the electronic conductive paths. The TEM image of the 400^{o}C treated Si/PAN composite shown in Fig. 5 confirms the existence of conductive carbon and will be discussed in greater depth later.

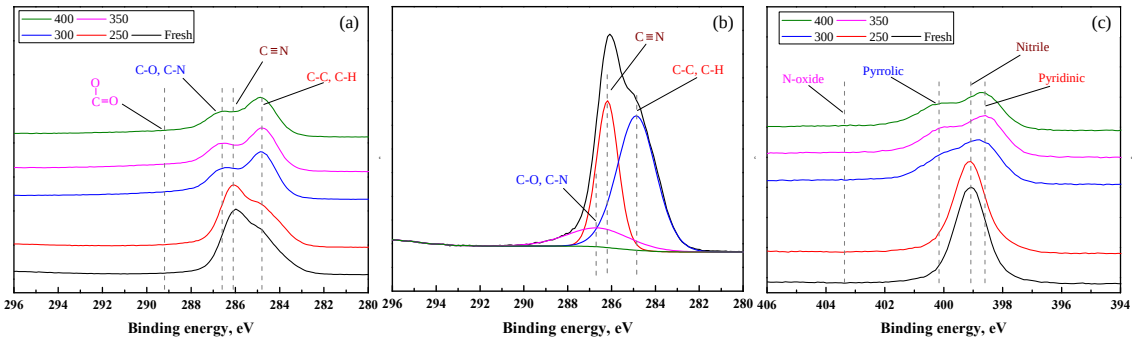

Figure 3.10 XPS spectra of Si/PAN composites (a) C1s (b) high resolution C1s of 250oC treated Si/PAN composite (c) N 1s

Table 3.3 Compositions of N sites (obtained by XPS) and I_D/I_G ratios of Si/PAN composite electrodes (obtained by Raman)

	Composition of N sites (%)				I_D/I_G
	Nitrile	Pyridinic	Pyrrolic	N-Oxide	
Fresh	100	0	0	0	**
250	63.7	26.8	9.6	0	3.37
300	0	54.6	39.3	6.0	3.41
350	0	48.8	43.4	7.8	3.48
400	0	48.5	43.7	7.8	3.46

The Raman spectra further confirm the presence of cyclized PAN in the oxidative pyrolyzed samples. As shown in Fig. 4, a single peak at around 520 cm^{-1}, which is attributed to Si, is present in the fresh Si/PAN composite. After heat treatment, broad peaks at 1370 cm^{-1} (D), 1590 cm^{-1} (G), 2720 cm^{-1} (2D), and 2950 cm^{-1} (D+G) emerge, suggesting the existence of cyclized PAN. A Gaussian-Lorentzian function is used to fit each peak. The relative intensity (I_D/I_G) which quantifies the degree of disorder in carbon materials is also summarized in Table 2. Unlike the work published by other research groups[157, 177], the I_D/I_G ratio does not decrease with increasing temperature. It remains nearly constant, especially with the Si/PAN composites treated at above 300oC, in which the remaining PAN are nearly all stabilized. The key difference is that the PAN or the PAN containing

composites in the aforementioned references were heat treated in an inert environment facilitating the formation of basal planes of graphitic layers when the temperature is increased, leading to a higher degree of order. In contrast, air is used in the present work. Instead of converting to a more ordered structure, the carbon is more likely to react with oxygen and leave the Si/PAN composites as CO and CO_2 with increasing temperature, resulting in a constant I_D/I_G ratio.

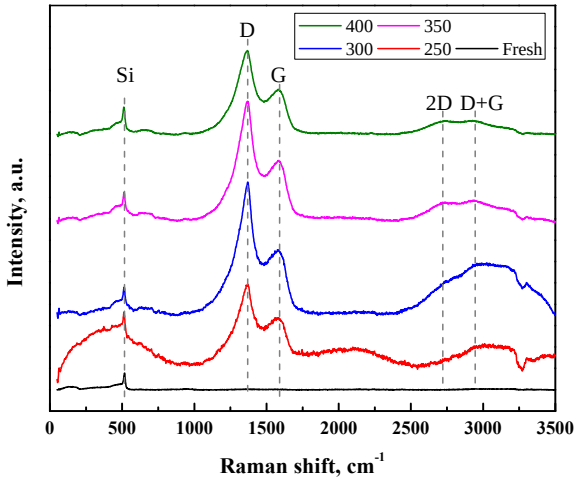

Figure 3.11 Raman spectra of Si/PAN composites

Shown in Fig. 3.12 is the TEM image of the 400^{o}C treated Si/PAN composite. A structure of Si particles embedded in the carbon matrix formed by stabilized PAN is observed. The distribution of all elements can be found in Fig. 3.13. Surprisingly, a considerable amount of onion-like carbon, which has an electrical conductivity comparable to carbon black[178], is detected (highlighted with the red ovals in Fig. 12(b)). These carbon-onions can help establish the electronic conductive paths throughout the electrode. The rest of the amorphous carbon may contribute to electronic conduction and act as the binder to hold the Si particles together during electrochemical cycling, leading to superior electrochemical performance of the Si/PAN composite.

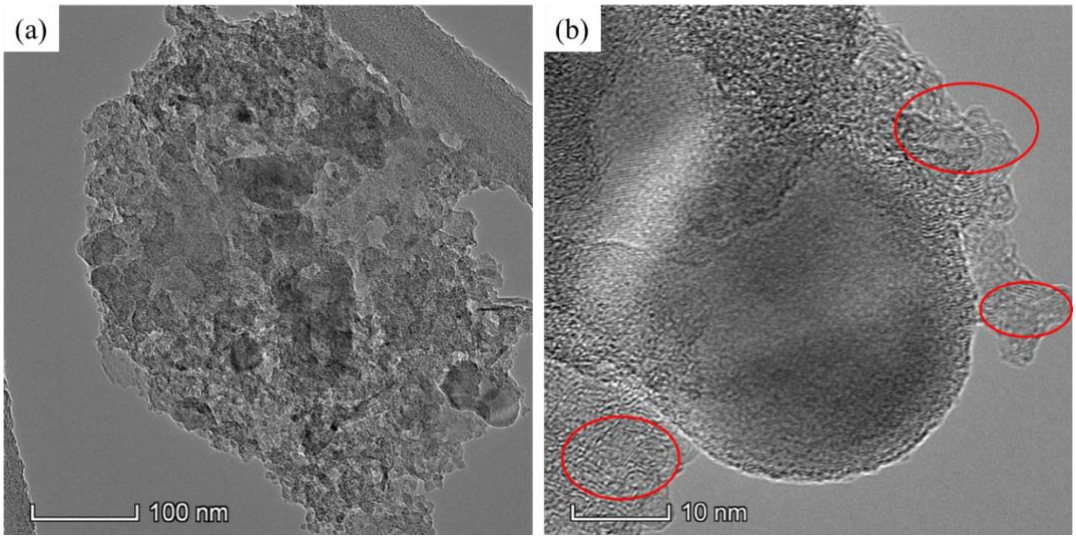

Figure 3.12 TEM images of 400oC treated Si/PAN composite electrode

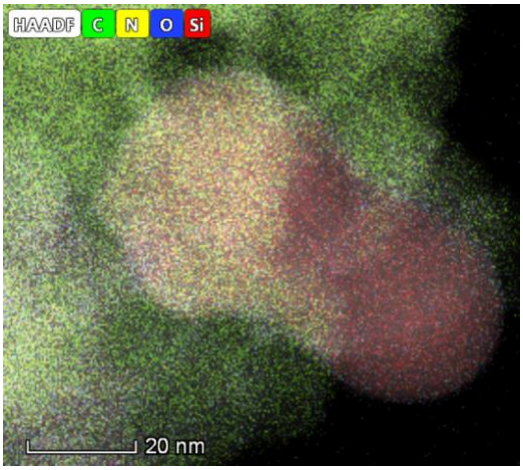

Figure 3.13 TEM elemental mapping of
Si/PAN composite electrode treated at 400oC

It is well established that polymeric binders play a crucial role in determining the electrochemical performance of Si electrodes. Mechanical resilience is believed to be one of the most important properties that is required for a binder to accommodate the huge volume expansion/contraction of Si and assure a good electrode performance. Yet, the mechanical properties of an effective binder or Si/binder composites, e.g. elastic modulus, hardness, and reversible deformation are still unclear. Here, we conducted nano-

indentation tests on the Si/PAN composites. The elastic moduli and hardness values, which are derived from the loading-unloading curves using an Oliver-Pharr method, are shown in Fig. 3.14. It is clear that the fresh and 250$_o$C treated Si/PAN composites have similar mechanical properties with much lower elastic moduli (E) and hardness values (H) than those treated at higher temperatures. TGA (Fig. S3), EDS (Table 1), and XPS (Fig. 3) results demonstrate that the concentration of each element and structure of PAN in the 250$_o$C treated Si/PAN composite does not change much from the fresh one. A similar mechanical property is thus a consequence of overall alike structures of these two samples. Nonetheless, the structural evolution of the Si/PAN composites heat treated at temperatures higher than 300$_o$C is much more complex. First, PAN starts to be burnt out from the composite (indicated by TGA (Fig. S4)), resulting in an increased mass percent of Si and thus an increment of electrode modulus and hardness. Second, the mechanical properties of PAN itself change with temperature. In the temperature range of 250$_o$C to 400$_o$C, the modulus of PAN could increase or remain constant with increasing temperature depending on the heating conditions[170]. Last, our previous work showed that the modulus and hardness of a porous electrode decrease with reduced porosity[179]. Recall the SEM images (Fig. 2) clearly show the porosity changes with increasing temperature, as a result, the mechanical properties should change accordingly. Coupling the effects of these three factors results in the modulus and hardness of the Si/PAN composites treated with higher temperatures similar to each other but considerably higher than the fresh and 250$_o$C treated ones.

The numbers inserted in Fig. 3.14 are the ratios between hardness and modulus (H/E), which according to Cheng et al.[180], is proportional to the ratio of reversible work

to total work from one indentation test. Typically, the larger this number, the bigger portion of the deformation during the indentation test is elastic. Evidently, the Si/PAN composites treated at temperatures higher than 300^{o}C have the same H/E ratio, which is much lower than either the fresh or the 250^{o}C treated samples, suggesting the Si/PAN composite is less "elastic" when the temperature exceeds 300^{o}C. In fact, many cracks with no apparent delamination are observed in all four types of electrodes after cycling (Fig. 3.15). Nevertheless, the composites treated at higher temperatures actually have better performance (Fig. 1), indicating that the elasticity of the Si/PAN composite treated with temperatures higher than 300^{o}C is likely to be sufficient to facilitate volume changes during electrochemical reactions. Similar to the findings with stiff binders and cracking behavior in Si composite electrodes [105, 108, 122], our results show that the stiff Si/PAN composites do not necessarily perform worse than the soft ones, the cracks in the composites caused by the expansion/contraction of Si particles with lithiation/delithiation may not negatively affect the electrochemical performance of Si electrodes. However, the exact correlation between the mechanical property of a Si composite electrode and the electrochemical performance should be further investigated.

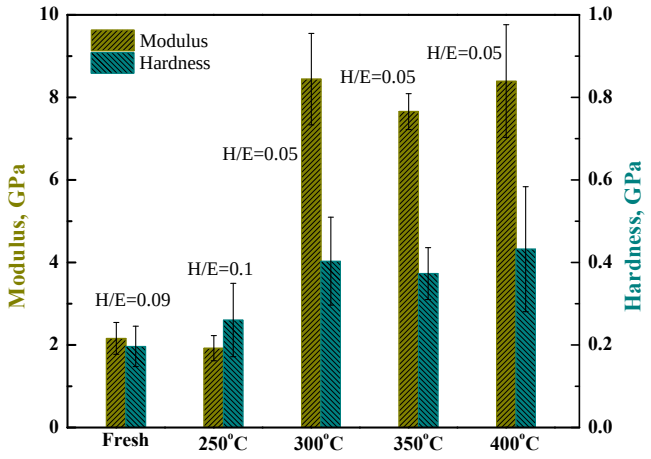

Figure 3.14 Elastic modulus and hardness of Si/PAN composites heat treated at different temperatures

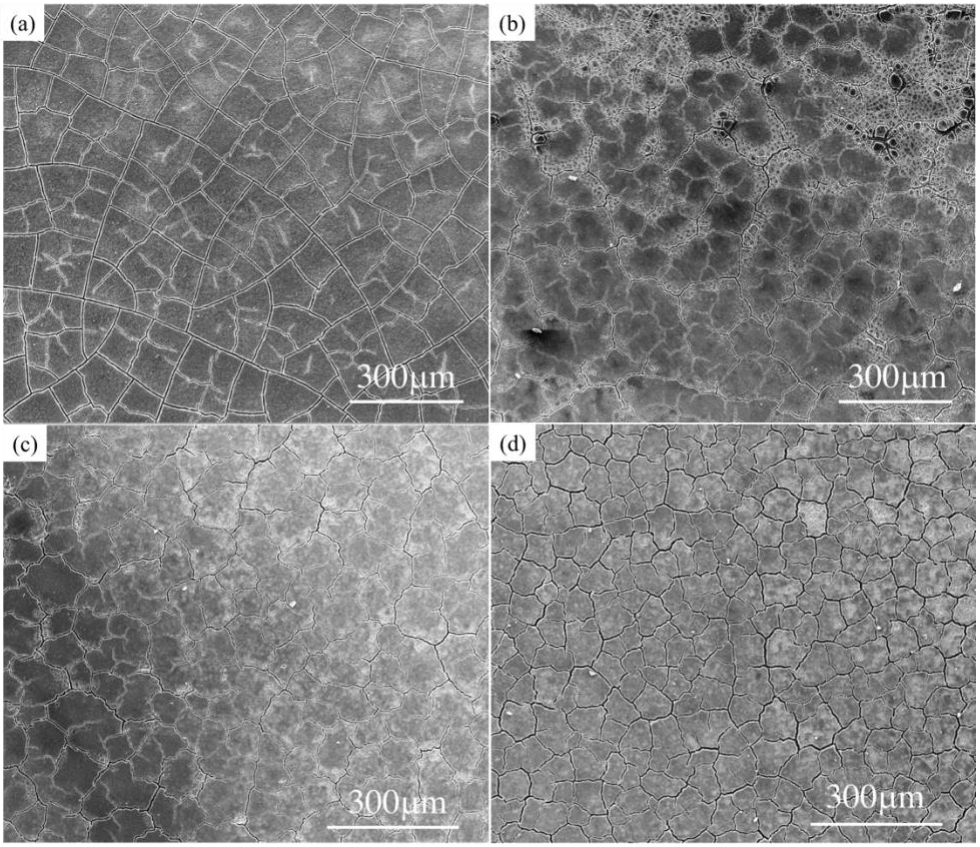

Figure 3.15 Surface morphology of Si/PAN composite electrodes after 100 cycling at C/3 (a) treated at 250oC, (b) treated at 300oC, (c) treated at 350oC, and (d) treated at 400oC

3.4 Conclusion

Si/PAN composites are successfully synthesized by oxidative pyrolysis of the composite with a temperature between 250 to 400^{o}C. The 400^{o}C treated Si/PAN composite when tested as the negative electrode in LIBs, showed excellent long term cycling performance as well as good high rate cycling ability. Structural, chemical, and mechanical studies showed that cyclization/stabilization of PAN occurred with oxidative pyrolysis, producing a matrix that is both electronically conducting and mechanically strong. Increasing temperature leads to an increasingly porous structure, higher degree of stabilization, and improved electronic conductivity. A synergetic effect of the structural, chemical, and mechanical properties enabled the 400^{o}C treated Si/PAN composite to deliver a discharge capacity of 1614 mAh/g at the 100th cycle. This facile method to synthesize Si comprised composite negative electrode may be applied to other Si/polymer systems to further improve the power/energy density of LIBs. In addition, carbon onion, one of the most promising members in the carbon family, that is commonly synthesized by graphitization of nanodiamonds at temperature as high as 1700^{o}C in an inert gas or vacuum[178], is detected in the 400^{o}C treated Si/PAN composite. Our findings may provide insight into producing carbon onions at much lower temperature consuming much less energy.

Chapter 4 Conclusions and future work

4.1 Conclusions

In my thesis research, the effects of adhesion/cohesion behavior, which is largely determined by polymeric binder, on the performance and durability of Si electrode are investigated by various techniques including peel tests, SEM, TEM, XRD, FTIR, XPS, and electrochemical cycling. A robust process of oxidative pyrolysis is proposed that may be used to fabricate high performance Si composite electrode for the next generation LIBs. The main conclusions are:

(1) PVDF adheres to Cu current collector better than sodium alginate (SA) whereas SA has a stronger interface with silicon than that between PVDF and silicon. Both Si/PVDF/CB and Si/SA/CB electrodes adhere strongly to the current collector to cause separation within the electrode layer during 180_o peel tests. However, mechanical property of binder and the adhesion of electrode layer to the current collector are not key parameters that determine the electrochemical performance of Si electrode. Instead, the binder-silicon interface influences the performance of Si electrode more.

(2) Because of the stronger binder-silicon interface in the Si/SA/CB electrode, the silicon particles are held together by the SA binder during lithiation/delithiation. As a result, the silicon particles could participate in the electrochemical reactions repeatedly to allow the Si/SA/CB electrode be cycled for more than 600 cycles when the lithiation capacity is limited to 900 mAh/g and deliver a nearly constant cut off voltage. Si/PVDF/CB electrode, on the other hand, cannot reach the lithiation limit after 20 cycles and shows a cut off voltage decreased to 0.01 V rapidly. The absence of a strong binder-silicon interface

is responsible for the poor performance. Because of the weak PVDF-silicon interface, silicon particles detach from the conductive matrix due to the huge volume expansion/contraction during charging/discharging and cannot form alloy with lithium after just a few cycles.

(3) Chemical analysis shows that covalent bonds do not form between PVDF(SA) and silicon. However, there is an oxide layer on the surface of the silicon particles. Thus, the origin of the strong SA-silicon interface is most likely the hydrogen bond formed between SA and the hydroxyl groups on the silicon surface.

(4) High performance Si/PAN composite electrodes can be fabricated by an robust oxidative pyrolysis process at temperature from 250 to 400^{o}C. During the heat treatment in air, originally linear PAN transforms into a cyclized structure that acts as both a binder and a conductive agent in the Si/PAN composite electrode. Simultaneously, PAN reacts with O_2 to create a porous structure in the electrode to allow electrolyte to filtrate in. As a result the 400^{o}C treated Si/PAN shows the best electrochemical performance with both low and high current density.

(5) Mechanically, the Si/PAN composite electrodes treated at higher temperatures are much stiffer than the untreated and low temperature treated ones. However, the electrochemical performance of the stiff Si/PAN composite electrode is actually better than the soft ones. In accordance with other reports, our results show that the mechanical properties of the Si composite electrode does not necessarily influence the electrochemical performance of the electrodes.

(6) Carbon onions, that are usually obtained by graphitizing nonodimonds at temperature as high as 1700^{o}C, are observed in the oxidative pyrolyzed Si/PAN composite

at 400^{o}C. This work may provide insights into producing carbon onions at much lower temperature using much less energy.

4.2 Future work

Based on the studies and results that have been reported in this thesis, some additional work that may help gain a better understanding of the working/failure mechanism to further improve the electrochemical performance and durabiity of Si-based electrodes are summarized here:

(1) It should be noted that both the adhesive and cohesive strength of Si electrode reported in chapter 2 are the strengths in freshly made samples. Namely, the strengths of the dried and uncycled electrodes. However, several research groups have reported that polymeric binder would swell in the organic electrolyte by absorbing solvent, resulting in the change of the mechanical property of binder itself and the stress field around electrode particles[109, 124, 181-184], which may develop a different binder-silicon interface than in the fresh electrodes. The adhesive/cohesive strength in the presence of electrolyte could, thus, change as well. In addition, the evolution of the binder-silicon interface with lithiation/dilithiation is unknown. The influence of the SEI layer on the cohesive strength also remains unclear. More work should be done to answer these questions to gain a thorough understanding of how polymeric binders affect the structure and performance of Si electrodes, which allows us to modify existing and/or design new binder systems to improve the performance and cycle life of Si-based electrode.

(2) The conditions that used in chapter 3 to fabricate Si-based composite are not optimized. Parameters, e.g., temperature, time duration during the heat treatment, gaseous environment, type of polymer, and mass ratio between Si and the polymer, can all be

optimized so that the performance of the electrodes can be further improved. Furthermore, alternative heating/pyrolyzing methods, such as ultraviolet, microwave, and plasma that may heat/pyrolyze the composite electrodes with shorter time and/or less energy, may be investigated to lower the cost of making high performance and durable Si-based composite electrodes.

Bibliography

[1] K. Brandt, Historical development of secondary lithium batteries.Solid State Ionics, 69 (1994) 173-183.
[2] Y. Nishi, The Development of Lithium Ion Secondary Batteries.The Chemical Record, 1 406-413.
[3] M.M.W. Thackeray, Christopher Isaacs, Eric D., Electrical energy storage for transportation—approaching the limits of, and going beyond, lithium-ion batteries.Energy & Environmental Science, 5 (2012) 7854.
[4] J.-M. Tarascon, M. Armand, Issues and challenges facing rechargeable lithium batteries.Nature, 414 (2001) 359-367.
[5] X. Jiagang, Investigation of the critical role of polymeric binders for silicon negative electrodes in lithium-ion batteries.(2016).
[6] L. Shen, Q. Che, H. Li, X. Zhang, Mesoporous NiCo2O4Nanowire Arrays Grown on Carbon Textiles as Binder-Free Flexible Electrodes for Energy Storage.Advanced Functional Materials, 24 (2014) 2630-2637.
[7] M. Al-Shroofy, Q. Zhang, J. Xu, T. Chen, A. Kaur, Y.-T. Cheng, Solvent-free dry powder coating process for low-cost manufacturing of LiNi1/3Mn1/3Co1/3O2 cathodes in lithium-ion batteries.Journal of Power Sources, 352 (2017) 187-193.
[8] J.C.B. Nupur Nikkan Sinha, R.J. Sanderson, J. Dahn, Comparative Studies of Hardware Corrosion at High Potentials in Coin-Type Cells with Non Aqueous Electrolytes.Journal of Electrochemical Society, 158 (2001) A1400-A1403.
[9] Kim Kinoshitaa, K. Zaghib, Negative electrodes for Li-ion batteries.Journal of Power Sources, 110 (2002) 416-423.
[10] K. Nobuhara, H. Nakayama, M. Nose, Nakanishi, Shinji Iba, Hideki, First-principles study of alkali metal-graphite intercalation compounds.Journal of Power Sources, 243 (2013) 585-587.
[11] P. Lian, X. Zhu, S. Liang, Z. Li, W. Yang, H. Wang, Large reversible capacity of high quality graphene sheets as an anode material for lithium-ion batteries.Electrochimica Acta, 55 (2010) 3909-3914.
[12] P. Guo, Song, Huaihe, X. Chen, Electrochemical performance of graphene nanosheets as anode material for lithium-ion batteries.Electrochemistry Communications, 11 (2009) 1320-1324.
[13] EunJoo Yoo, Jedeok Kim, Eiji Hosono, Haoshen Zhou, Tetsuichi Kudo, I. Honma, Large Reversible Li Storage of Graphene Nanosheet Families for Use in Rechargeable Lithium Ion Batteries.Nano letters, 8 (2008) 2277-2282.
[14] X. Xiao, P. Liu, J.S. Wang, M.W. Verbrugge, M.P. Balogh, Vertically aligned graphene electrode for lithium ion battery with high rate capability.Electrochemistry Communications, 13 (2011) 209-212.
[15] B.J. Landi, M.J. Ganter, C.D. Cress, R.A. DiLeo, R.P. Raffaelle, Carbon nanotubes for lithium ion batteries.Energy & Environmental Science, 2 (2009) 638.
[16] S.H. Ng, J. Wang, Z.P. Guo, J. Chen, G.X. Wang, H.K. Liu, Single wall carbon nanotube paper as anode for lithium-ion battery.Electrochimica Acta, 51 (2005) 23-28.
[17] S.W. Lee, N. Yabuuchi, B.M. Gallant, S. Chen, B.S. Kim, P.T. Hammond, Y. Shao-Horn, High-power lithium batteries from functionalized carbon-nanotube electrodes.Nat Nanotechnol, 5 (2010) 531-537.

[18] J. Jiang, Y. Li, J. Liu, X. Huang, C. Yuan, X.W. Lou, Recent advances in metal oxide-based electrode architecture design for electrochemical energy storage.Adv Mater, 24 (2012) 5166-5180.
[19] B. Koo, H. Xiong, M.D.P. Slater, V. B. Balasubramanian, M., P. Podsiadlo, C.S. Johnson, T. Rajh, E.V. Shevchenko, Hollow iron oxide nanoparticles for application in lithium ion batteries.Nano Lett, 12 (2012) 2429-2435.
[20] J. Chen, L. Xu, W. Li, X. Gou, a-Fe2O3 Nanotubes in Gas Sensor and Lithium-Ion Battery Applications.Advanced Materials, 17 (2005) 582-586.
[21] M.V. Reddy, T. Yu, C.H. Sow, Z.X. Shen, C.T. Lim, G.V. Subba Rao, B.V.R. Chowdari, α-Fe2O3 Nanoflakes as an Anode Material for Li-Ion Batteries.Advanced Functional Materials, 17 (2007) 2792-2799.
[22] S.A. Needham, G.X. Wang, H.K. Liu, Synthesis of NiO nanotubes for use as negative electrodes in lithium ion batteries.Journal of Power Sources, 159 (2006) 254-257.
[23] Q.L. Wu, J. Li, R.D. Deshpande, N. Subramanian, S.E.Y. Rankin, Fuqian , Y.-T. Cheng, Aligned TiO2 Nanotube Arrays As Durable Lithium-Ion Battery Negative Electrodes.The Journal of Physical Chemistry C, 116 (2012) 18669-18677.
[24] W.Y. Li, L.N. Xu, J. Chen, Co3O4 Nanomaterials in Lithium-Ion Batteries and Gas Sensors.Advanced Functional Materials, 15 (2005) 851-857.
[25] L. Zhou, D. Zhao, X.W. Lou, Double-shelled CoMn2O4 hollow microcubes as high-capacity anodes for lithium-ion batteries.Adv Mater, 24 (2012) 745-748.
[26] Y.P. Wu, E. Rahm, R. Holze, Carbon anode materials for lithium ion batteries.Journal of Power Sources, 114 (2003) 228-236.
[27] A.N. Dey, Electrochemical Alloying of Lithium in Organic Electrolytes.Journal of Electrochemical Society, 118 (1971) 1547-1549.
[28] C.M. Park, J.H. Kim, H. Kim, H.J. Sohn, Li-alloy based anode materials for Li secondary batteries.Chemical Society Revievs, 39 (2010) 3115-3141.
[29] Martin Winter, J.r.O. Besenhard, Electrochemical lithiation of tin and tin-based intermetallics and composites.Electrochemicala Acta, 45 (1999) 31-50.
[30] M.N. Obrovac, V.L. Chevrier, Alloy negative electrodes for Li-ion batteries.Chemical Reviews, 114 (2014) 11444-11502.
[31] J. Li, J.R. Dahn, An In Situ X-Ray Diffraction Study of the Reaction of Li with Crystalline Si.Journal of The Electrochemical Society, 154 (2007) A156.
[32] X.H. Liu, J.Y. Huang, In situ TEM electrochemistry of anode materials in lithium ion batteries.Energy & Environmental Science, 4 (2011) 3844.
[33] K. Rhodes, N. Dudney, E. Lara-Curzio, C. Daniel, Understanding the Degradation of Silicon Electrodes for Lithium-Ion Batteries Using Acoustic Emission.Journal of The Electrochemical Society, 157 (2010) A1354.
[34] R.A. Huggins, W.D. Nix, Decrepitation Model For Capacity Loss During Cycling of Alloys in Rechargeable Electrochemical Systems.International Journal of Ionics, 6 (2000) 57-63.
[35] C.K. Chan, H. Peng, G. Liu, K. McIlwrath, X.F. Zhang, R.A. Huggins, Y. Cui, High-performance lithium battery anodes using silicon nanowires.Nature Nanotechnology, 3 (2008) 31-35.
[36] Li-Feng Cui, Liangbing Hu, Jang Wook Choi, Y. Cui, Light-Weight Free-Standing Carbon Nanotube-Silicon Films for Anodes of Lithium Ion Batteries.ACS Nano, 4 (2010) 3671-3678.

[37] T. Song, J. Xia, J.H. Lee, D.H. Lee, M.S. Kwon, J.M. Choi, J. Wu, S.K. Doo, H. Chang, W.I. Park, D.S. Zang, H. Kim, Y. Huang, K.C. Hwang, J.A. Rogers, U. Paik, Arrays of sealed silicon nanotubes as anodes for lithium ion batteries.Nano Letters, 10 (2010) 1710-1716.
[38] A. Magasinski, P. Dixon, B. Hertzberg, A. Kvit, J. Ayala, G. Yushin, High-performance lithium-ion anodes using a hierarchical bottom-up approach.Nature Materials, 9 (2010) 353-358.
[39] J. Graetz, C.C. Ahn, R. Yazami, B. Fultz, Highly Reversible Lithium Storage in Nanostructured Silicon.Electrochemical and Solid-State Letters, 6 (2003) A194.
[40] I. Ryu, J.W. Choi, Y. Cui, W.D. Nix, Size-dependent fracture of Si nanowire battery anodes.Journal of the Mechanics and Physics of Solids, 59 (2011) 1717-1730.
[41] Xiao Hua Liu, Li Zhong, Shan Huang, Scott X. Mao, Ting Zhu, J.Y. Huang, Size-Dependent Fracture of Silicon Nanoparticles During Lithiation.ACS Nano, 6 (2012) 1522-1531.
[42] N. Liu, Z. Lu, J. Zhao, M.T. McDowell, H.W. Lee, W. Zhao, Y. Cui, A pomegranate-inspired nanoscale design for large-volume-change lithium battery anodes.Nature Nanotechnology, 9 (2014) 187-192.
[43] N. Liu, H. Wu, M.T. McDowell, Y. Yao, C. Wang, Y. Cui, A yolk-shell design for stabilized and scalable li-ion battery alloy anodes.Nano Letters, 12 (2012) 3315-3321.
[44] H. Wu, G. Chan, J.W. Choi, I. Ryu, Y. Yao, M.T. McDowell, S.W. Lee, A. Jackson, Y. Yang, L. Hu, Y. Cui, Stable cycling of double-walled silicon nanotube battery anodes through solid-electrolyte interphase control.Nature Nanotechnology, 7 (2012) 310-315.
[45] Z. Wen, G. Lu, S. Mao, H. Kim, S. Cui, K. Yu, X. Huang, P.T. Hurley, O. Mao, J. Chen, Silicon nanotube anode for lithium-ion batteries.Electrochemistry Communications, 29 (2013) 67-70.
[46] J.K. Yoo, J. Kim, Y.S. Jung, K. Kang, Scalable fabrication of silicon nanotubes and their application to energy storage.Advanced Materials, 24 (2012) 5452-5456.
[47] M. Ge, J. Rong, X. Fang, C. Zhou, Porous doped silicon nanowires for lithium ion battery anode with long cycle life.Nano Letters, 12 (2012) 2318-2323.
[48] X. Lu, T.D.G. Bogart, Meng , C.K. Wang, Brian A., In Situ TEM Observations of Sn-Containing Silicon Nanowires Undergoing Reversible Pore Formation Due to Fast Lithiation/Delithiation Kinetics.The Journal of Physical Chemistry C, 119 (2015) 21889-21895.
[49] L. Luo, H. Yang, P. Yan, J.J. Travis, Y. Lee, N. Liu, D.M. Piper, S.H. Lee, P. Zhao, S.M. George, J.G. Zhang, Y. Cui, S. Zhang, C. Ban, C.M. Wang, Surface-coating regulated lithiation kinetics and degradation in silicon nanowires for lithium ion battery.ACS Nano, 9 (2015) 5559-5566.
[50] Nian Liu, M.T.M. Liangbing Hu, Ariel Jackson, Y. Cui, Prelithiated Silicon Nanowires as an Anode for Lithium Ion Batteries.ACS Nano, 5 (2011) 6487-6493.
[51] M. Inaba, M.S. Haruta, Morihiro , T. Doi, Silicon Nano-flake Powder as an Anode for The Next Generation Lithium-ion Batteries: Current Status and Challenges.Electrochemistry, 85 (2017) 623-629.
[52] H. Kim, B. Han, J. Choo, J. Cho, Three-dimensional porous silicon particles for use in high-performance lithium secondary batteries.Angewandte Chemie International Edition, 47 (2008) 10151-10154.

[53] N. Lin, Y. Han, J. Zhou, K. Zhang, T. Xu, Y. Zhu, Y. Qian, A low temperature molten salt process for aluminothermic reduction of silicon oxides to crystalline Si for Li-ion batteries.Energy & Environmental Science, 8 (2015) 3187-3191.
[54] Z.W. Zhou, Y.T. Liu, X.M. Xie, X.Y. Ye, Aluminothermic reduction enabled synthesis of silicon hollow microspheres from commercialized silica nanoparticles for superior lithium storage.Chemical Communication, 52 (2016) 8401-8404.
[55] W.C. Cho, H.J. Kim, H.I. Lee, M.W. Seo, H.W. Ra, S.J. Yoon, T.Y. Mun, Y.K. Kim, J.H. Kim, B.H. Kim, J.W. Kook, C.Y. Yoo, J.G. Lee, J.W. Choi, 5L-Scale Magnesio-Milling Reduction of Nanostructured SiO2 for High Capacity Silicon Anodes in Lithium-Ion Batteries.Nano letters, (2016).
[56] H. Jia, P. Gao, J. Yang, J. Wang, Y. Nuli, Z. Yang, Novel Three-Dimensional Mesoporous Silicon for High Power Lithium-Ion Battery Anode Material.Advanced Energy Materials, 1 (2011) 1036-1039.
[57] K.H. Kim, D.J. Lee, K.M. Cho, S.J. Kim, J.K. Park, H.T. Jung, Complete magnesiothermic reduction reaction of vertically aligned mesoporous silica channels to form pure silicon nanoparticles.Scientific Report, 5 (2015) 9014.
[58] D. Chen, X. Mei, G. Ji, M. Lu, J. Xie, J. Lu, J.Y. Lee, Reversible lithium-ion storage in silver-treated nanoscale hollow porous silicon particles.Angewandte Chemie International Edition, 51 (2012) 2409-2413.
[59] L. Wu, H. Zhou, J.Z. Yang, Xiangyang Ren,, Yongpeng Nie, S. Yang Chen, Carbon coated mesoporous Si anode prepared by a partial magnesiothermic reduction for lithium-ion batteries.Journal of Alloys and Compounds, 716 (2017) 204-209.
[60] Y. Yu, L. Gu, C. Zhu, S. Tsukimoto, P.A. van Aken, J. Maier, Reversible storage of lithium in silver-coated three-dimensional macroporous silicon.Advanced Materials, 22 (2010) 2247-2250.
[61] Y. Zhao, X. Liu, H. Li, T. Zhai, H. Zhou, Hierarchical micro/nano porous silicon Li-ion battery anodes.Chemical Communication, 48 (2012) 5079-5081.
[62] M. Thakur, S.L.I. Sinsabaugh, M. J. , M.S. Wong, S.L. Biswal, Inexpensive method for producing macroporous silicon particulates (MPSPs) with pyrolyzed polyacrylonitrile for lithium ion batteries.Scientific Reports, 2 (2012) 795.
[63] T.Z. Jiang, Ruibo , Q. Yin, W. Zhou, Z.C. Dong, Natasha A. , Q. Wang, F. Omenya, M. Whittingham, Stanley, Morphology, composition and electrochemistry of a nano-porous silicon versus bulk silicon anode for lithium-ion batteries.Journal of Materials Science, 52 (2017) 3670-3677.
[64] M.P. Thakur, Roderick B. Nitta, Naoki , M.S. Isaacson, Steven L. , M.S.B. Wong, Sibani Lisa, Freestanding Macroporous Silicon and Pyrolyzed Polyacrylonitrile As a Composite Anode for Lithium Ion Batteries.Chemistry of Materials, 24 (2012) 2998-3003.
[65] J. Liu, D. Xue, Hollow Nanostructured Anode Materials for Li-Ion Batteries.Nanoscale Research Letters, 5 (2010) 1525-1534.
[66] Y. Yao, M.T. McDowell, I. Ryu, H. Wu, N. Liu, L. Hu, W.D. Nix, Y. Cui, Interconnected silicon hollow nanospheres for lithium-ion battery anodes with long cycle life.Nano Letters, 11 (2011) 2949-2954.
[67] S. Sampath, P. Maydannik, T. Ivanova, T. Homola, M. Sillanpää, Nagumothu, Rameshbabu, V. Alagan, Structural and morphological characterization of Al2O3 coated macro-porous silicon by atomic layer deposition.Thin Solid Films, 616 (2016) 628-634.

[68] L. Zong, Y. Jin, C. Liu, B. Zhu, X. Hu, Z. Lu, J. Zhu, Precise Perforation and Scalable Production of Si Particles from Low Grade Sources for High Performance Lithium Ion Battery Anodes.Nano Letters, (2016).
[69] W. He, H. Tian, F. Xin, W. Han, Scalable fabrication of micro-sized bulk porous Si from Fe–Si alloy as a high performance anode for lithium-ion batteries.Journal of Materials Chemistry A, 3 (2015) 17956-17962.
[70] L. Lin, X. Xu, C. Chu, M.K. Majeed, J. Yang, Mesoporous Amorphous Silicon: A Simple Synthesis of a High-Rate and Long-Life Anode Material for Lithium-Ion Batteries.Angewandte Chemie International Edition, 55 (2016) 14063-14066.
[71] D. Wang, D. Choi, J. Li, Z. Yang, Z. Nie, R. Kou, D. Hu, C. Wang, L.V. Saraf, J. Zhang, I.A. Aksay, J. Liu, Self-assembled TiO2-graphene hybrid nanostructures for enhanced Li-ion insertion.ACS Nano, 3 (2009) 907-914.
[72] L. Wang, Y. Yu, P.C. Chen, D.W. Zhang, C.H. Chen, Electrospinning synthesis of C/Fe3O4 composite nanofibers and their application for high performance lithium-ion batteries.Journal of Power Sources, 183 (2008) 717-723.
[73] H. Xia, M. Lai, L. Lu, Nanoflaky MnO2/carbon nanotube nanocomposites as anode materials for lithium-ion batteries.Journal of Materials Chemistry, 20 (2010) 6896.
[74] Zhong-Shuai Wu, Wencai Ren, Lei Wen, Libo Gao, Jinping Zhao, Zongping Chen, Guangmin Zhou, Feng Li, H. Cheng, Graphene Anchored with Co3O4 Nanoparticles as Anode of Lithium Ion Batteries with Enhanced Reversible Capacity and Cyclic Performance.ACS Nano, 4 (2010) 3187-3194.
[75] W.-M. Zhang, J.-S. Hu, Y.-G. Guo, S.-F. Zheng, L.-S. Zhong, W.-G. Song, L.-J. Wan, Tin-Nanoparticles Encapsulated in Elastic Hollow Carbon Spheres for High-Performance Anode Material in Lithium-Ion Batteries.Advanced Materials, 20 (2008) 1160-1165.
[76] Q. Xiao, Y. Fan, X. Wang, R. Susantyoko, Agung, Q. Zhang, A multilayer Si/CNT coaxial nanofiber LIB anode with a high areal capacity.Energy & Environ.mental Science, 7 (2014) 655-661.
[77] K. Fu, O. Yildiz, H. Bhanushali, Y. Wang, K. Stano, L. Xue, X. Zhang, P.D. Bradford, Aligned carbon nanotube-silicon sheets: a novel nano-architecture for flexible lithium ion battery electrodes.Advanced Materials, 25 (2013) 5109-5114.
[78] Y. Fan, Q. Zhang, Q. Xiao, X. Wang, K. Huang, High performance lithium ion battery anodes based on carbon nanotube–silicon core–shell nanowires with controlled morphology.Carbon, 59 (2013) 264-269.
[79] W. Wang, R. Epur, P.N. Kumta, Vertically aligned silicon/carbon nanotube (VASCNT) arrays: Hierarchical anodes for lithium-ion battery.Electrochemistry Communications, 13 (2011) 429-432.
[80] Wei Wang, P.N. Kumta, Nanostructured Hybrid Silicon/Carbon Nanotube Heterostructures: Reversible High-Capacity Lithium-Ion Anodes.ACS Nano, 4 (2010) 2233-2241.
[81] ShuLei Chou, Yue Zhao, JiaZhao Wang, ZhiXin Chen, HuaKun Liu, S.-X. Dou, Silicon/Single-Walled Carbon Nanotube Composite Paper as a Flexible Anode Material for Lithium Ion Batteries.Journal of Physical Chemistry C, 114 (2010) 15862–15867.
[82] P. Wu, H. Wang, Y. Tang, Y. Zhou, T. Lu, Three-dimensional interconnected network of graphene-wrapped porous silicon spheres: in situ magnesiothermic-reduction synthesis and enhanced lithium-storage capabilities.ACS Applied Materials & Interfaces, 6 (2014) 3546-3552.

[83] L. Xue, K. Fu, Y. Li, G. Xu, Y. Lu, S. Zhang, O.Z. Toprakci, Xiangwu, Si/C composite nanofibers with stable electric conductive network for use as durable lithium-ion battery anode.Nano Energy, 2 (2013) 361-367.
[84] T.Y. Okubo, Tomoyuki Saito, Morihiro Yodoya, Chihiro Kamei, Akika , M. Hirota, T. Takenaka, A. Tasaka, M. Inaba, Carbon Coating of Si Thin Flakes and Negative Electrode Properties in Lithium-Ion Batteries.Electrochemistry, 80 (2012) 720-724.
[85] D. Shao, D. Tang, Y. Mai, L. Zhang, Nanostructured silicon/porous carbon spherical composite as a high capacity anode for Li-ion batteries.Journal of Materials Chemistry A, 1 (2013) 15068.
[86] E. Biserni, M. Xie, R.S. Brescia, A. Hashempour, M. Movahed, P. , S.M.B. George, M. , A. Li Bassi, P. Bruno, Silicon algae with carbon topping as thin-film anodes for lithium-ion microbatteries by a two-step facile method.Journal of Power Sources, 274 (2015) 252-259.
[87] H. Wu, G. Zheng, N. Liu, T.J. Carney, Y. Yang, Y. Cui, Engineering empty space between Si nanoparticles for lithium-ion battery anodes.Nano Letters, 12 (2012) 904-909.
[88] K. Mizushima, P.C. Jones, P.J. Wiseman, J.B. Goodenough, LixCoO2 (0<x<1): A new cathod material for batteries of high energy density.Materials Research Bulletin, 15 (1980) 783-789.
[89] T. Zhang, D. Li, Z. Tao, J. Chen, Understanding electrode materials of rechargeable lithium batteries via DFT calculations.Progress in Natural Science: Materials International, 23 (2013) 256-272.
[90] H. XIA, Y.S. MENG, L. LU, G. CEDER, Electrochemical behavior and Li Diffusion study of LiCoO2 thin film electrodes.(2007).
[91] J.R. Dahn, Rechargeable LiNiO2/Carbon Cells.Journal of The Electrochemical Society, 138 (1991) 2207-2211.
[92] G. Vitins, K. West, Lithium Intercalation into Layered LiMnO2.Journal of The Electrochemical Society, 144 (1997) 2587-2592.
[93] H. Arai, M.S. Tsuda, Keiichi Hayashi, Masahiko Sakurai, Yoji, Thermal Reactions Between Delithiated Lithium Nickelate and Electrolyte Solutions.Journal of The Electrochemical Society, 149 (2002) A401.
[94] H.S.P. Seong Ju Hwang, J.H. Choy, Evolution of Local Structure around Manganese in Layered LiMnO2 upon Chemical and Electrochemical Delithiation/Relithiation.Chemistry of Materials, 12 (2000) 1818-1826.
[95] T.O.Y. Makimura, Layered Lithium Insertion Material of LiNi1/2Mn1/2O2:A Possible Alternative to LiCoO2 for Advanced Lithium-Ion Batteries.Chemistry Letters, 30 (2001) 744-745.
[96] N. Yabuuchi, T. Ohzuku, Novel lithium insertion material of LiCo1/3Ni1/3Mn1/3O2 for advanced lithium-ion batteries.Journal of Power Sources, 119-121 (2003) 171-174.
[97] N.V. Kosova, E.T. Devyatkina, V.V. Kaichev, Optimization of Ni2+/Ni3+ ratio in layered Li(Ni,Mn,Co)O2 cathodes for better electrochemistry.Journal of Power Sources, 174 (2007) 965-969.
[98] Y.K. Sun, Z. Chen, H.J. Noh, D.J. Lee, H.G. Jung, Y. Ren, S. Wang, C.S. Yoon, S.T. Myung, K. Amine, Nanostructured high-energy cathode materials for advanced lithium batteries.Nature Materials, 11 (2012) 942-947.
[99] H.-J.Y. Noh, Sungjune, C.S.S. Yoon, Yang-Kook, Comparison of the structural and electrochemical properties of layered Li[NixCoyMnz]O2 (x = 1/3, 0.5, 0.6, 0.7, 0.8 and

0.85) cathode material for lithium-ion batteries.Journal of Power Sources, 233 (2013) 121-130.
[100] W.I.F.D. M.M. Thackeray, P.G. Bruce, J.B. Goodenough, LITHIUM INSERTION INTO MANGANESE SPINELS.Materials Research Bulletin, 18 (1983) 461-472.
[101] T. Ohzuku, R.J. Brodd, An overview of positive-electrode materials for advanced lithium-ion batteries.Journal of Power Sources, 174 (2007) 449-456.
[102] K. Zaghib, J. Shim, A. Guerfi, P. Charest, K.A. Striebel, Effect of Carbon Source as Additives in LiFePO4 as Positive Electrode for Lithium-Ion Batteries.Electrochemical and Solid-State Letters, 8 (2005) A207.
[103] H.W. Wang, Rui , L. Sun, Z.Z. Liu, Yixing , Y. Zhu, Mechanical and tribological characteristics of carbon nanotube-reinforced polyvinylidene fluoride (PVDF)/epoxy composites.RSC Advances, 6 (2016) 45636-45644.
[104] M.T. Jeena, J.I. Lee, S.H. Kim, C. Kim, J.Y. Kim, S. Park, J.H. Ryu, Multifunctional molecular design as an efficient polymeric binder for silicon anodes in lithium-ion batteries.ACS Applied Materials Interfaces, 6 (2014) 18001-18007.
[105] J. Li, R.B. Lewis, J.R. Dahn, Sodium Carboxymethyl Cellulose.Electrochemical and Solid-State Letters, 10 (2007) A17.
[106] W.-R. Liu, M.-H. Yang, H.-C.C. Wu, S. M. , N.-L. Wu, Enhanced Cycle Life of Si Anode for Li-Ion Batteries by Using Modified Elastomeric Binder.Electrochemical and Solid-State Letters, 8 (2005) A100.
[107] N.S.S. Hochgatterer, M. R. Koller, S. , P.R.W.h. Raimann, T. , C. Wurm, M. Winter, Silicon/Graphite Composite Electrodes for High-Capacity Anodes: Influence of Binder Chemistry on Cycling Stability.Electrochemical and Solid-State Letters, 11 (2008) A76.
[108] A.Z. Magasinski, B. , I.H. Kovalenko, B. Burtovyy, R. Huebner, C. F. , T.F. Fuller, I. Luzinov, G. Yushin, Toward efficient binders for Li-ion battery Si-based anodes: polyacrylic acid.ACS Applied Materials Interfaces, 2 (2010) 3004-3010.
[109] H.-K.K. Park, Byung-Seon Oh, Eun-Suok, Effect of high adhesive polyvinyl alcohol binder on the anodes of lithium ion batteries.Electrochemistry Communications, 13 (2011) 1051-1053.
[110] J. Xu, Q. Zhang, Y.-T. Cheng, High Capacity Silicon Electrodes with Nafion as Binders for Lithium-Ion Batteries.Journal of The Electrochemical Society, 163 (2015) A401-A405.
[111] I.Z. Kovalenko, Bogdan Magasinski, Alexandre Hertzberg, Benjamin Milicev, Zoran Burtovyy, Ruslan Luzinov, Igor Yushin, Gleb, A Major Constituent of Brown Algae for Use in High-Capacity Li-Ion Batteries.Science, 334 (2011) 75-79.
[112] J. Hu, Y. Wang, D. Li, Y.-T. Cheng, Effects of adhesion and cohesion on the electrochemical performance and durability of silicon composite electrodes.Journal of Power Sources, 397 (2018) 223-230.
[113] Y. Wang, L. Lv, J. Wang, D. Yan, B. Geng, Z. Wu, R. Zhuo, Influence of microstructure on electrochemical properties of Si/C multilayer thin-film anodes deposited using a sputtering method.Materials Letters, 160 (2015) 210-212.
[114] J.R. Szczech, S. Jin, Nanostructured silicon for high capacity lithium battery anodes.Energy & Environmental Scicience, 4 (2011) 56-72.
[115] Y.-X. Wang, S.-L. Chou, J.H. Kim, H.-K. Liu, S.-X. Dou, Nanocomposites of silicon and carbon derived from coal tar pitch: Cheap anode materials for lithium-ion batteries with long cycle life and enhanced capacity.Electrochimica Acta, 93 (2013) 213-221.

[116] J.H. Ryu, J.W. Kim, Y.-E. Sung, S.M. Oh, Failure Modes of Silicon Powder Negative Electrode in Lithium Secondary Batteries.Electrochemical and Solid-State Letters, 7 (2004) A306.
[117] L.Y.E. Beaulieu, K. W. Turner, R. L. , L.J. Krause, J.R. Dahn, Colossal Reversible Volume Changes in Lithium Alloys.Electrochemical and Solid-State Letters, 4 (2001) A137.
[118] A.A. Benjamin Hertzberg, Gleb Yushin, Deformations in Si-Li Anodes Upon Electrochemical Alloying in Nano-Confined Space.Journal of the American Chemical Society, 132 (2010) 8548-8549.
[119] S.D. Beattie, D. Larcher, M. Morcrette, B. Simon, J.M. Tarascon, Si Electrodes for Li-Ion Batteries—A New Way to Look at an Old Problem.Journal of The Electrochemical Society, 155 (2008) A158.
[120] Y. Sun, N. Liu, Y. Cui, Promises and challenges of nanomaterials for lithium-based rechargeable batteries.Nature Energy, 1 (2016) 16071.
[121] Z.C. Chen, L. , J.R. Dahn, Large-volume-change electrodes for Li-ion batteries of amorphous alloy particles held by elastomeric tethers.Electrochemistry Communications, 5 (2003) 919-923.
[122] J. Xu, L. Zhang, Y. Wang, T. Chen, M. Al-Shroofy, Y.T. Cheng, Unveiling the Critical Role of Polymeric Binders for Silicon Negative Electrodes in Lithium-Ion Full Cells.ACS Applied Materials Interfaces, 9 (2017) 3562-3569.
[123] Min Ling, Yanan Xu, Hui Zhao, Xingxing Gu, Jingxia Qiu, Sheng Li, X.S. Mingyan Wu, Cheng Yanc,, Gao Liu, S. Zhang, Dual-functional Gum Arabic Binder for Silicon Anodes in Lithium Ion Batteries.Nano Energy, 12 (2015) 178-185.
[124] L. Chen, X. Xie, J. Xie, K. Wang, J. Yang, Binder effect on cycling performance of silicon/carbon composite anodes for lithium ion batteries.Journal of Applied Electrochemistry, 36 (2006) 1099-1104.
[125] S.Y. Komaba, Naoaki Ozeki, Tomoaki, Z.-J.S. Han, Keiji, H.K. Yui, Yasushi Miura, Takashi, Comparative Study of Sodium Polyacrylate and Poly(vinylidene fluoride) as Binders for High Capacity Si–Graphite Composite Negative Electrodes in Li-Ion Batteries.The Journal of Physical Chemistry C, 116 (2012) 1380-1389.
[126] M.H. Ryou, J. Kim, I. Lee, S. Kim, Y.K. Jeong, S. Hong, J.H. Ryu, T.S. Kim, J.K. Park, H. Lee, J.W. Choi, Mussel-inspired adhesive binders for high-performance silicon nanoparticle anodes in lithium-ion batteries.Advanced Materials, 25 (2013) 1571-1576.
[127] L. Zhang, L. Zhang, L. Chai, P. Xue, W. Hao, H. Zheng, A coordinatively cross-linked polymeric network as a functional binder for high-performance silicon submicro-particle anodes in lithium-ion batteries.Journal of Materials Chemistry A, 2 (2014) 19036-19045.
[128] K. Kierzek, Influence of Binder Adhesion Ability on the Performance of Silicon/Carbon Composite as Li-Ion Battery Anode.Journal of Materials Engineering and Performance, 25 (2016) 2326-2330.
[129] W.W. Haselrieder, B. Bockholt, H. , A. Diener, S. Höft, A. Kwade, Measuring the coating adhesion strength of electrodes for lithium-ion batteries.International Journal of Adhesion and Adhesives, 60 (2015) 1-8.
[130] S. Lee, Molecular Dynamics Study of the Separation Behavior at the Interface between PVDF Binder and Copper Current Collector.Journal of Nanomaterials, 2016 (2016) 1-12.

[131] S. Ben Slama, M. Hajji, H. Ezzaouia, Crystallization of amorphous silicon thin films deposited by PECVD on nickel-metalized porous silicon.Nanoscale Res Lett, 7 (2012) 464.
[132] M.H. Marouan Khalifa, Hatem Ezzaouia, Purification of silicon powder by the formation of thin porous layer followed byphoto-thermal annealing.Nanoscale Res. Lett., 7 (2012) 444-447.
[133] V. Hernández-Morales, R. Nava, Y.J. Acosta-Silva, S.A. Macías-Sánchez, J.J. Pérez-Bueno, B. Pawelec, Adsorption of lead (II) on SBA-15 mesoporous molecular sieve functionalized with –NH2 groups.Microporous and Mesoporous Materials, 160 (2012) 133-142.
[134] S.K. Parida, S. Dash, S. Patel, B.K. Mishra, Adsorption of organic molecules on silica surface.Adv Colloid Interface Sci, 121 (2006) 77-110.
[135] N. BETZ, A. LE MOEL, E. BALANZAT, J. M. RAMILLON, Z J. IJIMOTTE, J. P. CALLAS, C. JASKIEROWICZ, A FTIR Study of PVDF Irradiated by Means of Swift Heavy Ions.J. Polym. Sci. B, 32 (1994) 1493-1502.
[136] C. Pigliacelli, A. D'Elicio, R. Milani, G. Terraneo, G. Resnati, F. Baldelli Bombelli, P. Metrangolo, Hydrophobin-stabilized dispersions of PVDF nanoparticles in water.Journal of Fluorine Chemistry, 177 (2015) 62-69.
[137] X.-K. Lin, X. Feng, L. Chen, Y.-P. Zhao, Characterization of temperature-sensitive membranes prepared from poly(vinylidene fluoride)-graft-poly(N-isopropylacrylamide) copolymers obtained by atom transfer radical polymerization.Frontiers of Materials Science in China, 4 (2010) 345-352.
[138] J. Guo, C. Wang, A polymer scaffold binder structure for high capacity silicon anode of lithium-ion battery.Chemical Communication, 46 (2010) 1428-1430.
[139] D. Munao, J.W.M.V. van Erven, M. , E.K. Garcia-Tamayo, E. M., Role of the binder on the failure mechanism of Si nano-composite electrodes for Li-ion batteries.Journal of Power Sources, 196 (2011) 6695-6702.
[140] J. Yoon, D.X. Oh, C. Jo, J. Lee, D.S. Hwang, Improvement of desolvation and resilience of alginate binders for Si-based anodes in a lithium ion battery by calcium-mediated cross-linking.Physical Chemistry Chemical Physics, 16 (2014) 25628-25635.
[141] D. Liu, Y. Zhao, R. Tan, L.-L. Tian, Y. Liu, H. Chen, F. Pan, Novel conductive binder for high-performance silicon anodes in lithium ion batteries.Nano Energy, 36 (2017) 206-212.
[142] Zhen-Ji Han, S.H. Naoaki Yabuuchi, Takeo Sasaki, Shinichi Komaba, Cross-Linked Poly(acrylic acid) with Polycarbodiimide as Advanced Binder for Si/Graphite Composite Negative Electrodes in Li-Ion Batteries.ECS Electrochemistry Letters, 2 (2013) A17-A20.
[143] D.M. Piper, J.J. Travis, M. Young, S.B. Son, S.C. Kim, K.H. Oh, S.M. George, C. Ban, S.H. Lee, Reversible high-capacity Si nanocomposite anodes for lithium-ion batteries enabled by molecular layer deposition.Adv Mater, 26 (2014) 1596-1601.
[144] Z.-L. Xu, Y. Gang, M.A. Garakani, S. Abouali, J.-Q. Huang, J.-K. Kim, Carbon-coated mesoporous silicon microsphere anodes with greatly reduced volume expansion.Journal of Materials Chemistry A, 4 (2016) 6098-6106.
[145] J. Guo, A. Sun, X. Chen, C. Wang, A. Manivannan, Cyclability study of silicon–carbon composite anodes for lithium-ion batteries using electrochemical impedance spectroscopy.Electrochimica Acta, 56 (2011) 3981-3987.
[146] A.K. Roy, M. Zhong, M.G. Schwab, A. Binder, S.S. Venkataraman, Z. Tomovic, Preparation of a Binder-Free Three-Dimensional Carbon Foam/Silicon Composite as

Potential Material for Lithium Ion Battery Anodes.ACS Appl Mater Interfaces, 8 (2016) 7343-7348.
[147] Ying Li, Yujie Sun, Guanjie Xu, Yao Lu, Shu Zhang, Leigang Xue, Jess S. Jur, X. Zhang, Tuning electrochemical perfrmance of Si-based amodes for lithium-ion batteries by employing atomic layer deposition.Journal of Materials Chemistry A, 2 (2014) 11417-11425.
[148] Y. Tong, Z. Xu, C. Liu, G.a. Zhang, J. Wang, Z.G. Wu, Magnetic sputtered amorphous Si/C multilayer thin films as anode materials for lithium ion batteries.Journal of Power Sources, 247 (2014) 78-83.
[149] R. Yi, F. Dai, M.L. Gordin, S. Chen, D. Wang, Micro-sized Si-C Composite with Interconnected Nanoscale Building Blocks as High-Performance Anodes for Practical Application in Lithium-Ion Batteries.Advanced Energy Materials, 3 (2013) 295-300.
[150] T. Chen, Q. Zhang, J. Pan, J. Xu, Y. Liu, M. Al-Shroofy, Y.T. Cheng, Low-Temperature Treated Lignin as Both Binder and Conductive Additive for Silicon Nanoparticle Composite Electrodes in Lithium-Ion Batteries.ACS Applied Materials Interfaces, 8 (2016) 32341-32348.
[151] N. Dimov, S. Kugino, M. Yoshio, Mixed silicon–graphite composites as anode material for lithium ion batteries.Journal of Power Sources, 136 (2004) 108-114.
[152] I.-s. Kim, G.E. Blomgren, P.N. Kumta, Si–SiC nanocomposite anodes synthesized using high-energy mechanical milling.Journal of Power Sources, 130 (2004) 275-280.
[153] L. Ji, X. Zhang, Electrospun carbon nanofibers containing silicon particles as an energy-storage medium.Carbon, 47 (2009) 3219-3226.
[154] L. Ji, K.-H. Jung, A.J. Medford, X. Zhang, Electrospun polyacrylonitrile fibers with dispersed Si nanoparticles and their electrochemical behaviors after carbonization.Journal of Materials Chemistry, 19 (2009) 4992.
[155] L. Ji, X. Zhang, Fabrication of porous carbon/Si composite nanofibers as high-capacity battery electrodes.Electrochemistry Communications, 11 (2009) 1146-1149.
[156] X. Fan, L. Zou, Y.-P. Zheng, F.-Y. Kang, W.-C. Shen, Electrospinning Preparation of Nanosilicon/Disordered Carbon Composite as Anode Materials in Li-Ion Battery.Electrochemical and Solid-State Letters, 12 (2009) A199.
[157] D.M. Piper, T.A. Yersak, S.-B. Son, S.C. Kim, C.S. Kang, K.H. Oh, C. Ban, A.C. Dillon, S.-H. Lee, Conformal Coatings of Cyclized-PAN for Mechanically Resilient Si nano-Composite Anodes.Advanced Energy Materials, 3 (2013) 697-702.
[158] J.S. Thomas A. Yersak, Ziying Wang, J.W. Daniel Estrada, Se-Hee Lee, Y.S.M. Michael J. Sailor, Preparation of Mesoporous Si@PAN Electrodes for Li-Ion Batteries via the In-Situ Polymerization of PAN.ECS Electrochemistry Letters, 4 (2015) A33-A36.
[159] R. B. Mathur, O. P. Bahl, J. Mittal, A new approach to thermal stabilisation of PAN fibers.Carbon, 30 (1992) 657-663.
[160] J. Mital, O. P. Bahl, R.B. Mathur, single step carbonization and graphitization of highly stabilized PAN fibers.Carbon, 35 (1997) 1196-1197.
[161] A. Gupta, I.R. Harrison, New aspects in the oxidative stabilization of PAN-based carbon fibers.Carbon, 34 (1996) 1427-1445.
[162] E. Fiter, D.J. Muller, The influence of oxygen on the chemical reactions during stabilization of PAN as carbon fiber precusor.Carbon, 13 (1975) 63-69.
[163] O. P. Bahl, L.M. Manocha, Characterization of oxidised PAN fibers.Carbon, 12 (1974) 417-423.

[164] Q. Wang, X. Sun, D. He, J. Zhang, Preparation and study of carbon nano-onion for lithium storage.Materials Chemistry and Physics, 139 (2013) 333-337.
[165] Y. Zheng, P. Zhu, Carbon nano-onions: large-scale preparation, functionalization and their application as anode material for rechargeable lithium ion batteries.RSC Advances, 6 (2016) 92285-92298.
[166] F.-D. Han, B. Yao, Y.-J. Bai, Preparation of Carbon Nano-Onions and Their Application as Anode Materials for Rechargeable Lithium-Ion Batteries.The Journal of Physical Chemistry C, 115 (2011) 8923-8927.
[167] B.E. Deal, A.S. Grove, General Relationship for the Thermal Oxidation of Silicon.Journal of Applied Physics, 36 (1965) 3770-3778.
[168] L. Reich, Polymer Degradation by Differential Thermal Analysis Techniques.Journal of Polymer Science Macromolecular Reviews, 3 (1968) 49-112.
[169] E.D. Weil, Carbon fibers, 2nd edition by J. B. Donnet and R. C. Bansal, Marcel Dekker, New York (1990).Polymers for Advanced Technologies, 3 (1992) 47-47.
[170] A. Gupta, I.R. Harrison, New aspects in the oxidative stabilization of PAN-based carbon fibers: II.Carbon, 35 (1997) 809-818.
[171] R. B. MATHUR, O. P. BAHL, J. MITTAL, A NEW APPROACH TO THERMAL STABILISATION OF PAN FIBRES.Carbon, 30 (1992) 657-663.
[172] X. Huang, Fabrication and Properties of Carbon Fibers.Materials, 2 (2009) 2369-2403.
[173] T. Van Khai, H.G. Na, D.S. Kwak, Y.J. Kwon, H. Ham, K.B. Shim, H.W. Kim, Significant enhancement of blue emission and electrical conductivity of N-doped graphene.Journal of Materials Chemistry, 22 (2012) 17992.
[174] R. B. Mathur, O. P. Bahl, J. Mittal, K.C. Nagpal, Structure of thermally stabilized PAN fibers.Carbon, 29 (1991) 1059-1061.
[175] J. Mittal, O. P. Bahl, R. B.Mathur, N.K. Sandle, IR studies f PAN fibers thermally stabilized at elecvated temperatures.Carbon, 32 (1994) 1133-1136.
[176] M. Jing, C. Wang, Q. Wang, Y. Bai, B. Zhu, Chemical structure evolution and mechanism during pre-carbonization of PAN-based stabilized fiber in the temperature range of 350–600°C.Polymer Degradation and Stability, 92 (2007) 1737-1742.
[177] S. Lee, J. Kim, B.-C. Ku, J. Kim, H.-I. Joh, Structural Evolution of Polyacrylonitrile Fibers in Stabilization and Carbonization.Advances in Chemical Engineering and Science, 02 (2012) 275-282.
[178] M. Zeiger, N. Jäckel, V.N. Mochalin, V. Presser, Review: carbon onions for electrochemical energy storage.Journal of Materials Chemistry A, 4 (2016) 3172-3196.
[179] Yikai Wang, Z. Qinglin, Dawei Li, , Jiazhi Hu, Jiagang Xu, X.X. Dingyign Dang, Yang-tse Cheng, Mechanical property evolution of silicon composite electrodes stuied by environmental nanoindentation.Advanced Energy Materials, 8 (2018) 1702578.
[180] Y.-T. Cheng, C.-M. Cheng, Scaling, dimensional analysis, and indentation measurements.Materials Science and Engineering: R: Reports, 44 (2004) 91-149.
[181] J. Lopez, Z. Chen, C. Wang, S.C. Andrews, Y. Cui, Z. Bao, The Effects of Cross-Linking in a Supramolecular Binder on Cycle Life in Silicon Microparticle Anodes.ACS Appl Mater Interfaces, 8 (2016) 2318-2324.
[182] D. Shin, H. Park, U. Paik, Cross-linked poly(acrylic acid)-carboxymethyl cellulose and styrene-butadiene rubber as an efficient binder system and its physicochemical effects

on a high energy density graphite anode for Li-ion batteries.Electrochemistry Communications, 77 (2017) 103-106.
[183] J.M. Foster, X. Huang, M. Jiang, S.J. Chapman, B. Protas, G. Richardson, Causes of binder damage in porous battery electrodes and strategies to prevent it.Journal of Power Sources, 350 (2017) 140-151.
[184] M. Yoo, C.W. Frank, S. Mori, S. Yamaguchi, Effect of poly(vinylidene fluoride) binder crystallinity and graphite structure on the mechanical strength of the composite anode in a lithium ion battery.Polymer, 44 (2003) 4197-4204.

Vita

Education

University of Kentucky, 2015-2019

University of Science and Technology Beijing, Master of Science, 2012-2015

University of Science and Technology Beijing, Bachelor of Science, 2008-2012

Publications

[1] Jiazhi Hu, Yikai Wang, Dawei Li, and Yang-Tse Cheng, "Effects of adhesion and cohesion on the electrochemical performance and durability of silicon composite electrodes." *Journal of Power Sources*, 397: 223-230 (2018)

[2] Ming Wang, Jiazhi Hu, Yikai Wang, and Yang-Tse Cheng, "The influence of polyvinylidene fluoride (PVDF) binder properties on $LiNi_{0.22}Co_{0.33}Mn_{0.33}O_2$ (NMC) electrodes made by a dry-powder-coating process." *Journal of the Electrochemical Society*, 166(10): A2151-A2157 (2019)

[3] Yan Sun, Xiaowen Zhan, Jiazhi Hu, Yikai Wang, Shuang Gao, Yuhua Shen, and Yang-Tse Cheng, "Improving ionic conductivity with bimodal-sized Li7La3Zr2O12 fillers for composite polymer electrolytes." *ACS Applied Materials Interfaces*, 11(13): 12467-12475 (2019)

[4] Yikai Wang, Dingying Dang, Dawei Li, Jiazhi Hu, and Yang-Tse Cheng, "Influence of polymeric binders on mechanical properties and microstructure evolution of silicon composite electrodes during electrochemical cycling." *Journal of Power Sources*, 425(15): 170-178 (2019)

[5] Yikai Wang, Qinglin Zhang, Dawei Li, Jiazhi Hu, Jiagang Xu, Dingying Dang, Xingcheng Xiao, and Yang-Tse Cheng. "Mechanical property evolution of silicon composite electrodes

studied by environmental nanoindentation." *Advanced Energy Materials* 8 (10): 1702578 (2018)

[6] Dawei Li, Yikai Wang, Jiazhi Hu, Bo Lu, Dingying Dang, Junqian Zhang, and Yang-Tse Cheng. "Role of polymeric binders on mechanical behavior and cracking resistance of silicon composite electrodes during electrochemical cycling." *Journal of Power Sources* 387: 9-15 (2018)

[7] Dawei Li, Yikai Wang, Jiazhi Hu, Bo Lu, Yang-Tse Cheng, and Junqian Zhang. "*In situ* measurement of mechanical property and stress evolution in a composite silicon electrode." *Journal of Power Sources* 366: 80-85 (2017)

[8] Tao Chen, Jiazhi Hu, Long Zhang, Jie Pan, Yiyang Liu, and Yang-Tse Cheng. "High performance binder-free SiO_x/C composite LIB electrode made of SiO_x and lignin." *Journal of Power Sources* 362: 236-242 (2017)

Paper under review

[1] Jiazhi Hu, Andrew W Meyer, Xiasong Huang, and Yang-Tse Cheng, "Oxidative pyrolysis of Si/polyacrylonitrile composites as an unconventional approach to fabricate high performance lithium ion battery negative electrodes." *Submitted to the journal Carbon*

Patent

[1] "*Methods of making high performance electrodes*," Xiaosong Huang, Jiazhi Hu, and Yang-Tse Cheng, submitted a US patent application jointly with General Motors.